UC Davis

Civil & Environmental Engineering

Title

Impact of bidirectional seismic shearing on the volumetric response of sand deposits

Permalink

https://escholarship.org/uc/item/9mm29952

Authors

Reyes, Andres

Adinata, James

Taiebat, Mahdi

Peer reviewed
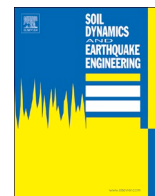
Impact of bidirectional seismic shearing on the volumetric response of sand deposits

Check for updates

Andrés Reyes, James Adinata, Mahdi Taiebat*

Department of Civil Engineering, University of British Columbia, Vancouver, BC, Canada

A R T I C L E   I N F O

Keywords:
Bidirectional seismic shearing
Liquefaction
Numerical modeling
Seismic site response

A B S T R A C T

Numerical simulation results of dry and saturated sand deposits subjected to both unidirectional and bidirectional seismic shearing were carried out and compared to quantify the increase of shear-induced volumetric response during shaking. The engineering demand parameters quantifying such response during the shaking events were considered to be the surface settlement for the dry deposits, and the depth-averaged peak excess pore water pressure and thickness of the liquefied layer for the saturated deposits. The numerical simulations made use of a three-dimensional continuum, coupled, dynamic, finite-difference platform and an anisotropic bounding surface plasticity constitutive model. Results of a series of centrifuge tests on saturated level ground sand deposits subjected to bidirectional shearing were used to validate the model capabilities for capturing the volumetric response of sand deposits. Over 1000 simulations were carried out in this study on homogeneous sand deposits with different densities and subjected to ground motions applied as uni- and bidirectional shearing. The dry models exhibited an 80% increase of surface settlement and in the saturated models depth-averaged peak excess pore water pressure ratios were up to 60% higher. Moreover, for the loose to medium dense 30 m-deep uniform deposits, the liquefied sand layers were in average 5–6 m thicker. These outcomes highlight the need to account for bidirectional seismic shearing when predicting the shear-induced volumetric response of sand deposits and related damaging phenomena such as liquefaction or seismic-induced settlement, among others. Furthermore, the simulation results shown the necessity for defining optimal ground motion intensity measures to characterize and scale ground motions for bidirectional shearing.

1. Introduction

Earthquake excitations have a multidirectional nature, constantly changing their amplitude and orientation. This loading feature induces intricate patterns of stress-strain behavior when the resulting waves travel through soil deposits. Fig. 1 shows the horizontal acceleration time-histories and acceleration orbit of the 1995 Kobe Earthquake recorded at the Shin-Osaka station, where loading irregularities and evolving shearing direction is revealed. Applying such horizontal components simultaneously rather than only one is likely to increase the volumetric response, as acknowledged since the 1970's through experimental studies. Specifically, Pyke et al. [1] and Seed et al. [2] conducted unidirectional (UD) and bidirectional (BD) shaking table tests on dry samples of Monterey No. 0 sand with relative densities (D_r) of 60% subjected to circular and earthquake-like loading paths, and depicted that BD shearing increased settlement up to 100% when compared to UD shearing. Furthermore, associated pore water pressure estimated using the Martin et al. [3] model suggested that the cyclic

shear ratio (CSR) required to cause liquefaction, or cyclic resistance ratio (CRR), was 10%–20% smaller under BD shearing. Fig. 2 illustrates the main outcomes of the above-mentioned studies. These early findings have shaped the development of simplified procedures that account for BD shearing to estimate seismic-induced settlement in dry [e.g., 4,5], and saturated [e.g., 6] level-ground sand deposits.

Years later, BD cyclic simple shear tests under undrained conditions were conducted by Ishihara and Yamazaki [7] using samples of Fuji River sand, who reported that CRR obtained under BD shearing were 30% lower than under UD shearing. Ishihara and Nagase [8] used Japanese earthquakes recordings to expand the former database, using Fuji River sand samples with D_r of 45%, 70% and 95%. The results disclosed that the added demand caused by BD shearing was not influenced by the level of D_r, as also noted recently by Jones and Sadrekarimi [9] using sinusoidal-type waveforms on samples of Fraser River sand. Kammerer et al. [10] completed a set of BD cyclic simple shear tests on fully saturated samples of Monterey No. 0/30 sand using several types of loading patterns. It was found that the CRR decrease of
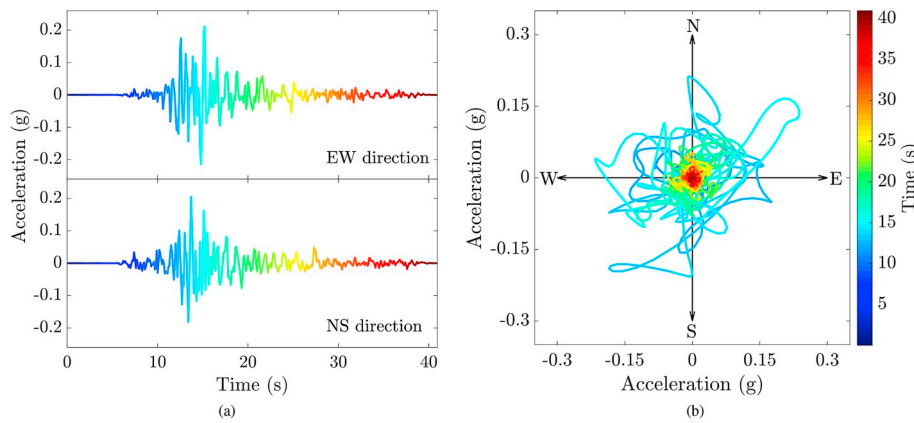

Fig. 1. Horizontal recordings of the 1995 Kobe earthquake at the Shin-Osaka station: (a) acceleration time-histories and (b) acceleration orbit (data from PEER Strong Motion Database [64]).
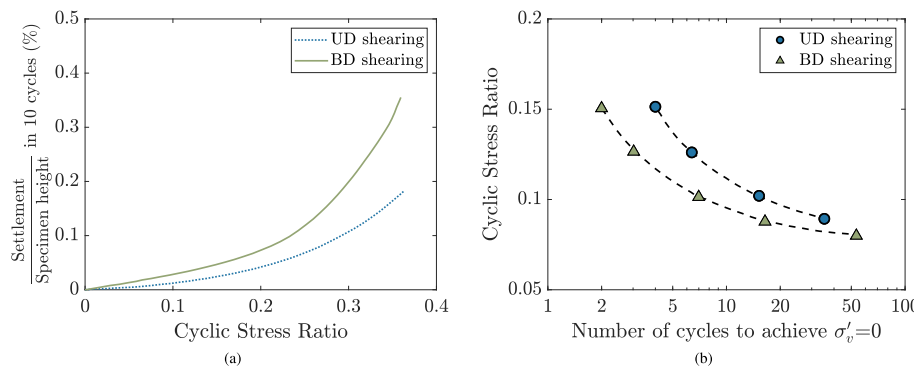

Fig. 2. Results from UD and BD shaking table tests on dry samples of Monterey No. 0: (a) settlement and (b) cyclic stress ratio (reproduced from Pyke et al. [1] and Seed et al. [2]).

10%–20% identified by Seed et al. [2] can overestimate liquefaction resistance under BD shearing. Moreover, it was identified that an excess pore water pressure ratio near or equal to 1 is not a requirement to achieve a liquefaction-like behavior during BD shearing: values as low as 0.7 were observed to be associated with the development of large shear strains. Bhaumik et al. [11] conducted UD and BD cyclic simple shear tests on dry samples of clean Ottawa 40/70 sand. Their results for $D_r \approx 50\%$ and 85% subjected to circular and figure-8 type shearing paths suggested that the increase of volumetric strain caused by BD over UD shearing varies between 50% and 200%, showing a wider range than the level reported by Pyke et al. [1] for Monterey No. 0 sand.

Based on centrifuge testing, Su and Li [12] investigated the response of a loose saturated level ground Toyoura sand deposit when subjected to UD and BD shear loading. By using sinusoidal-type waveforms as input, they observed an increase of excess pore water pressure and post-shaking settlement of 20% and 10%, respectively. More recently, El Shafee et al. [13,14] and Cerna-Diaz et al. [15] conducted similar tests on Nevada 120 and Ottawa 40/70 sand deposits, respectively. While El Shafee et al. [13,14] used synthesized motions to simulate the phase-time history of real earthquakes, Cerna-Diaz et al. [15] employed actual ground motion recordings with different levels of intensity. These studies showed that the increase in excess pore water pressure response during BD shearing may depend on the D_r of the sand deposit, and that it can be as much as 100% higher than during UD shearing for the case of dense sands.

Nie et al. [16] used a continuum-based numerical analysis approach to gain insight on the impact of BD shearing on dry sands. They used the computer program SUMDES [17] along with a double hardening bounding surface sand model [18–20], and focused on studying the seismic compression of element-level numerical models of dry Silica No. 2 sand by subjecting them to UD and BD seismic shearing. They

concluded that the rise of seismic compression caused by BD over UD shearing ranged from 50% to 130%. Furthermore, they showed that this increase was related to the level of D_r: the higher the density, the larger the impact of BD shearing. El Shamy and Abdelhamid [21] used a discrete element numerical analysis to examine the response of saturated granular deposits subjected to BD and UD sinusoidal-type motions. They made use of coupled lattice Boltzmann method discrete element simulations, which allowed them to present detailed acceleration time-histories and stress and strain loops. Their study revealed that BD shearing not only induced higher generation of excess pore water pressure but that it also led to a thicker layer of liquefied material (i.e., excess pore water pressure ratio close to 1) than UD shearing. Moreover, the resulting post-shaking settlement was shown to increase up to 30% as a consequence of BD shearing.

Most of the above research has made possible to foster our understanding on the behavior of saturated sands under BD shearing. However, while some of them highlight its importance on the shear-induced volumetric response of sand deposits [e.g., 13], others suggest that its effects are not significant [e.g., 12]. These contradictory observations can be attributed to the different levels of D_r, shear amplitudes/intensities (e.g., CSR, peak acceleration, Arias intensity), and shearing patterns (e.g., circular, figure-8, earthquake-like) employed in such studies. Moreover, existing simplified procedures to estimate seismic-induced settlements have not been updated in light of the recent experimental evidence. Consequently, there is a clear need for revisiting such procedures based on validated numerical methods that can consider the potential increase of volumetric response in BD shearing.

To thoroughly quantify the effect of BD seismic shearing on the volumetric response of sand, this paper presents a numerical database derived by performing non-linear site response analyses for UD and BD

shaking on homogeneous dry and fully saturated loose to dense sand deposits. The numerical analyses were conducted in a three-dimensional (3D) finite difference computer program along with an anisotropic bounding surface plasticity model for sands and focused on simulating the shear-induced volumetric response during shaking. Consequently, post-shaking settlements were not considered in this study. Localized and discontinuous phenomena such as ejecta, that can further contribute to settlement [22], were not accounted for either. The performance of the constitutive model was first assessed by validating its predictive capabilities against a set of centrifuge tests of saturated level ground sand deposits subjected to BD shearing. Following the validation, the development of the numerical database and the study the impact of BD seismic shearing relied on the constitutive model capacity for simulating shear-induced volumetric response during shaking. Therefore, for the case of the dry deposits, surface settlement was considered as performance index. On the other hand, excess pore water pressure response and the change of the thickness of liquefied layer were used for the saturated case. The motions used as input consisted of non-scaled earthquake recordings selected to cover a wide range of intensity measures and applied as UD and BD shearing at the base of the numerical model. The results of the analyses revealed the relevance of accounting for BD seismic shearing and the need for it to be considered in the volumetric response of sand deposits. Moreover, additional simulations conducted using a separate set of scaled ground motions showed the importance of defining optimal ground motion intensity measures associated to both UD and BD shaking.

2. Numerical framework

This section introduces the computational platform used in all the simulations throughout this paper, followed by a detailed description of the constitutive model.

2.1. Computational platform

The numerical simulations were completed in the finite difference computer platform $FLAC^{3D}$ [23], which uses an explicit time-integration scheme to model the dynamic response of 3D continuous media. In this program, the continuous media is replaced by a discrete-equivalent domain in which forces and displacements involved in the analysis are concentrated at the nodes of the 3D mesh used in representing the domain. Each zone or element of the mesh is comprised by a number of constant strain-rate subzones of tetrahedral shape whose vertices coincide with the ones of the zone. Solid-pore fluid interaction in this platform is based on the well-established coupled formulations of poromechanics originated by Biot [24] and extended by Detournay and Cheng [25]. The numerical scheme for the coupled formulation in fully saturated media relies on a fluid continuity equation, which relates fluid flow to changes in pore pressure and volumetric strain. Solving this equation requires a series of steps involving fluid flow loops followed by mechanical loops to maintain equilibrium state. The fluid flow loops calculate changes in pore pressure while the mechanical loops address the changes in volumetric strain due to the adjustment of effective stress induced by the fluid flow loops. A built-in isotropic fluid model is used in this study for simulation of the mechanical response of the pore fluid.

Adinata [26] carried out a detailed verification study on the reliability of this numerical platform for simulation of wave propagation and solid-pore fluid interaction. This included evaluation of important details such as adequate spatial (Δh) and temporal (Δt) discretizations, Rayleigh damping parameters and treatment of boundary conditions, for simulation of such problems, by comparing the performance of the computer program against a number of close-form solutions of one-dimensional (1D) elastic wave propagation problems through single and double phase media. For 1D propagation of shear waves in 8-node brick elements, the element size Δh should be less than about 1/10 of the

smallest wavelength ($\lambda_{\min}$) of interest, which can be estimated as $V_{\min}/f_{\max}$, i.e., the ratio of the minimum wave velocity of the medium and the maximum excitation frequency. On other hand, the simulation time step Δt should prevent the fastest traveling wave from reaching two consecutive nodes at the same time, which otherwise would violate a fundamental property of wave propagation, leading to instability of numerical solution [27]. The adequate time step can be first estimated as the ratio of Δh and maximum wave velocity of the medium, or $\Delta h/V_{\max}$. However, this estimation should be further reduced by a factor of 5–10 to prevent possible numerical instabilities caused by the explicit time-integration scheme of the computational platform. Rayleigh damping coefficients should be selected in order to cover a frequency range between the first and third modal frequencies of the deposit, as recommended by Kwok et al. [28]. This criteria was verified against analytical solutions defined in time [29] and frequency [30] domains. Finally, for modeling of level ground sites with a rigid base, where 1D wave propagation is expected, the imposed boundary conditions consist of fixing the vertical displacements at the base of the domain and tying the side nodes at each elevation. These criteria were used throughout the validation section and the development of the numerical database.

2.2. Constitutive model

Studying multidirectional shaking in saturated media by means of a numerical approach requires the use of a constitutive model capable of modeling the complexities of wave propagation in a 3D setting. In particular, the soil constitutive model used in the corresponding simulations needs to comply with a number of requirements such as being formulated in the multiaxial space, having mechanisms for reproducing soil stiffness and strength, coupling between volumetric and deviatoric responses, among others [31]. Based on these requirements, the constitutive model selected for this study follows the basic premises of the original two-surface plasticity model developed by Manzari and Dafalias [32] and its sequel by Dafalias and Manzari [33] with a useful fabric-dilatancy quantity, entering the realm of what was later on named SANISAND class of models [34]. The modeling approach is based on bounding surface plasticity with kinematic hardening of the yield surface (YS) and critical state soil mechanics concepts, allowing for a unified description at any pressure and density by the same set of model constants. The former studies [32,33] represent the core of the constitutive model, and a number of subsequent works [19,34–37] include different extensions and constitutive features that can be added to the original framework. To involve fewer model parameters and for simplicity, the version of Dafalias and Manzari [33] together with an overshooting correction scheme as described in Dafalias and Taiebat [37] has been considered as the reference soil constitutive model, and it is referred to with the generic name of SANISAND hereafter. Table 1 summarizes the constitutive equations of the version of SANISAND used in this study. Model implementation and testing in FLAC^{3D} was completed by Barrero [38]. This implementation has been already employed and compared against another one in a different numerical platform [39] in the comprehensive study by Ramirez et al. [40]. The verification of the model implementation is not repeated here. An extensive description of the base model can be found in the foregoing references, and here only a brief descriptive outline is presented.

SANISAND was developed within the frameworks of critical state soil mechanics and bounding surface plasticity. The major constitutive ingredients are the use of bounding and dilatancy surfaces, abbreviated here as BS and DS, respectively, in the multiaxial deviatoric stress space, generalizing the peak stress ratio and dilatancy stress ratio (phase transformation line slope) in p-q space, respectively. Both surfaces are made functions of the state parameter ψ [41] such that at critical state where $\psi = 0$, the surfaces collapse onto the fixed critical state surface that generalizes the critical state stress ratio $q/p = M$ in p-q space. Such dependence of BS on ψ allows the description of the softening response for denser than critical samples, an idea first

Table 1

Multiaxial constitutive equations in the SANISAND version used in this study [after 33,37].

Formulation constituents	Multiaxial equations	Constants
Critical state	$e_c = e_0 - \lambda (p_c/p_{atm})^\xi$	e_0, λ, ξ
	$\boldsymbol{\alpha}_\theta^c = \sqrt{2/3}\,[g(\theta, c)M - m]\boldsymbol{n}$	M, c
Elastic deviatoric strain increment	$\dot{\boldsymbol{e}}^e = d\boldsymbol{s}/2G$	
	$G = G_0 p_{atm}\,[(2.97 - e)^2/(1 + e)](p/p_{atm})^{1/2}$	G_0
Elastic volumetric strain increment	$\dot{\varepsilon}_v^e = dp/K$	
	$K = 2(1 + \nu)G/3(1 - 2\nu)$	ν
Yield surface	$f = [(\boldsymbol{s} - p\boldsymbol{\alpha})\colon (\boldsymbol{s} - p\boldsymbol{\alpha})]^{1/2} - \sqrt{2/3}\,pm = 0$	m
Plastic deviatoric strain increment	$\dot{\boldsymbol{e}}^p = \langle L\rangle \boldsymbol{R}'$	
	$K_p = (2/3)ph(\boldsymbol{\alpha}_\theta^b - \boldsymbol{\alpha})\colon \boldsymbol{n}$	
	$\boldsymbol{\alpha}_\theta^b = \sqrt{2/3}\,[g(\theta, c)M\exp(-n^b\psi) - m]\boldsymbol{n}$	n^b
	$h = b_0/(\boldsymbol{\alpha} - \boldsymbol{\alpha}_{in})\colon \boldsymbol{n}$	
	$b_0 = G_0 h_0 (1 - c_h e)(p/p_{atm})^{-1/2}$	h_0, c_h
Plastic volumetric strain increment	$\dot{\varepsilon}_v^p = \langle L\rangle D$	
	$D = A_d(\boldsymbol{\alpha}_\theta^d - \boldsymbol{\alpha})\colon \boldsymbol{n}$	
	$\boldsymbol{\alpha}_\theta^d = \sqrt{2/3}\,[g(\theta, c)M\exp(n^d\psi) - m]\boldsymbol{n}$	n^d
	$A_d = A_0(1 + \langle \boldsymbol{z}\colon \boldsymbol{n}\rangle)$	A_0
Fabric-dilatancy tensor update	$\dot{\boldsymbol{z}} = -c_z \langle \dot{\varepsilon}_v^p\rangle (z_{max}\boldsymbol{n} + \boldsymbol{z})$	c_z, z_{max}
Back-stress ratio tensor update	$\dot{\boldsymbol{\alpha}} = \langle L\rangle (2/3)h(\boldsymbol{\alpha}_\theta^b - \boldsymbol{\alpha})$	
Overshooting correction	$\boldsymbol{r}_{in}^{(i+1)} = m\boldsymbol{r}_{in}^{(i-1)} + (1 - m)\boldsymbol{r}^{(i)}$	
	$m = \langle 1 - (e_{eq}^{p(i)}/\bar{e}_{eq}^p)^n\rangle$	$\bar{e}_{eq}^p, n$

promoted by Wood et al. [42]. But even more important is the dependence of DS on ψ, first introduced by Manzari and Dafalias [32], because it is the underlying reason why the model can simulate the response of both dense and loose samples with same set of constants. Moreover, the model is able to capture the mean effective stress reduction due to the gradual increase of pore water pressure during cyclic loading under undrained conditions. The plastic modulus and dilatancy of the model are controlled by two parameters symbolized by h_0 and A_0, respectively. To better capture the sand response in cyclic loading, the contraction tendency during reverse loading following a dilation phase is enhanced by a fabric-dilatancy tensor, which accounts for the fabric changes during plastic dilation with evidences in microscopic studies. This reinforces the pore water pressure build up towards the liquefaction state, and allows the model to capture the butterfly shape of stress path as observed in the experiments.

SANISAND has been proven successful in reproducing the monotonic and pre-liquefaction cyclic response of sands for a wide range of pressures and densities under UD shearing in both element and centrifuge testing [e.g., 33,40,43–45]. Regarding BD cyclic shearing, Yang et al. [31] presented a detailed evaluation of the model against a large database of BD cyclic shear tests conducted on Monterey No. 0/30 sand by Kammerer et al. [10]. Their model calibration was based on the UD loading laboratory tests of Riemer [46], Wu [47], and Kammerer et al. [10]. Then, their evaluation, specifically designed to examine the performance of the model in the element level, revealed that SANISAND was successful in capturing excess pore water pressure built up for a number of loading paths of BD shearing without any further recalibration.

The above studies have shown the model strengths in capturing volumetric or pore water pressure response of sand subjected to cyclic shearing before and after the onset of liquefaction at near zero effective stresses. Furthermore, they have also demonstrated that SANISAND adequately represents the cyclic shear stress-strain response of sands in undrained loading as the mean effective stress reaches a value close to zero. However, after this point, the stress-strain loops of the model appear to lock-up within a few cycles, preventing it to capture the increase of large shear strains with the number of cycles as seen in the experiments. This is essentially attributed to a shortcoming of the model in capturing the shear strains at the near zero level of effective stress where the material is in its temporary *liquefied* regime before it goes to dilation and regain its strength. For this reason, the present study essentially focuses on the shear-induced *volumetric* response of the model during shaking.

3. Validation of Constitutive Model

A validation process assesses the degree to which the model can accurately represent the real behavior of a material from a rather physical or mechanical perspective, and is typically conducted with respect of the intended use of the constitutive model, which in this case is the modeling of shear-induced volumetric response of sand deposits during BD shearing. For this purpose, considering existing assessments of the constitutive model performance against UD shearing laboratory and centrifuge tests and BD cyclic shear tests, model validation is extended here by introducing its evaluation against relatively recent BD shearing centrifuge tests of saturated sand deposits; such centrifuge tests are currently limited in the literature. Table 2 presents the
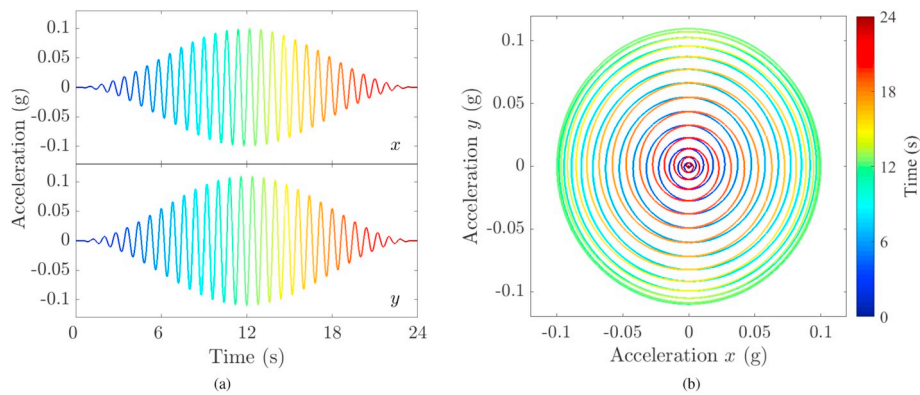
Table 2

Summary of centrifuge tests results used for validation.

Sand type	D_r	Motion	Loading pattern	Peak acceleration (g)		Reference
				x	y	
Toyoura	40%	1	Circular	0.10	0.11	Su and Li [12]
	40%	2	Circular	0.19	0.19	Su et al. [48]
Nevada	45%	3	Earthquake-like	0.10	0.10	El Shafee et al. [13]
	75%					El Shafee et al. [14]

Fig. 3. Target horizontal (a) acceleration time-histories and (b) acceleration orbit of motion 1 as described by Su and Li [12] and used in BD shearing centrifuge tests on Toyoura sand.

summary of the tests chosen for validation, which were conducted on two types of sand, different levels of D_r and a variety BD shearing patterns, covering a range of scenarios relevant to the objectives of this study.

The validation focused on assessing model performance against the volumetric response of the centrifuge tests, namely, in terms of excess pore water pressure and surface settlement during shaking. Consequently, reduction of effective stresses rather than accumulation of shear strains was the main focus of the validation. Large shear strain development after at the onset of liquefaction, i.e., near zero effective stress, and post-shaking excess pore water pressure dissipation and settlement were not evaluated in this study. The performance assessment of the constitutive model is assessed against a number of centrifuge tests subjected to bidirectional base shearing. All the testing measurements and simulation results are presented in the prototype scale unless specified otherwise.

3.1. Bidirectional shaking of Toyoura sand

3.1.1. Description of the centrifuge tests

Su and Li [12] and Su et al. [48] reported results of a series of BD shearing centrifuge tests conducted in the biaxial hydraulic shaker available at the Hong Kong University of Science and Technology (HKUST) centrifuge facility. The tests were performed on 16 m-deep Toyoura sand deposits, air pluviated to achieve an initial $D_r= 40\%$ and saturated with de-aired water under vacuum conditions. In order to minimize the effect of the boundaries of the container, the centrifuge tests made use of a rounded laminar box. Su [49] presented a detailed description of the shaker, instrumentation and testing program. Their centrifuge tests basically consisted on varying the loading conditions, particularly, the peak accelerations of the base input motions. Two of these were selected for the validation study, each one subjected to a different BD shearing motion, and labeled here as motion 1 and 2. Both of these share the same target loading pattern but differ in their peak acceleration along the x and y directions. Fig. 3 illustrates the x and y components of input acceleration time-histories, and the acceleration orbit of motion 1 as described in Su and Li [12]. Table 2 details the peak accelerations for each component for motions 1 and 2. The experimental results used for validation were the excess pore water pressure ratio (r_u) time-histories, peak excess pore water pressure (Δu_{peak}) depth profiles and surface settlement time-history, all during shaking.

3.1.2. Numerical simulations

The numerical model used to simulate these centrifuge tests consisted of a 16 m-deep 3D soil column. SANISAND parameters used to capture Toyoura sand response in the centrifuge tests were chosen from the calibration presented by Taiebat et al. [44], which was based on the monotonic and constant-p cyclic triaxial tests conducted by Verdugo

and Ishihara [50] and Pradhan et al. [51] for the same material used in the centrifuge tests. In this study, this calibration was updated to account for the overshooting correction and for the evolution of fabric dilatancy experienced during undrained cyclic loading in element tests. Specifically, results from the undrained cyclic torsional tests on Toyoura sand by Zhang et al. [52] were used to guide the calibration of parameters z_{max} and c_z, which control the fabric dilatancy tensor in SANISAND. The authors acknowledge that the Toyoura sand batch employed by Verdugo and Ishihara [50] and Pradhan et al. [51] ($D_{50} = 0.17$ mm, $e_{\max}= 0.977$ and $e_{\min}= 0.597$) appears to be slightly different from the batch of sand used by Zhang et al. [52] ($D_{50} = 0.18$ mm, $e_{\max}= 0.973$ and $e_{\min}= 0.635$). Consequently, the latter tests were merely used to calibrate the model for an adequate development of fabric dilatancy, as illustrated in Fig. 4, where the simulated dilation-contraction behavior is similar to the pattern of the experiment until the onset of liquefaction. The calibrated model parameters on the basis of these elements tests were used with no further adjustment in the simulation of the centrifuge tests.

Hydraulic conductivity used in the simulations considered the standard scaling coefficient for centrifuge testing as well as an additional scaling factor to account for the *agitation* phenomenon. Considering this latter scaling factor is consistent with the approach is used in Su [49] and Su and Li [12] to mimic the increase of hydraulic conductivity of liquefied soil in centrifuge tests that use water, as extensively reported in and/or discussed by Scott [53], Hushmand et al. [54], Ishihara [55], Kim et al. [56], Shahir et al. [57], Wang et al. [58] and others. Back-calculating from their own experimental results, Su [49] determined that an *agitation* scaling factor was necessary to adequately simulate the excess pore water pressure response recorded in their centrifuge tests. For this purpose, Su [49] reported a flow velocity-hydraulic gradient plot from which the scaling factor could be derived. This approach was then used in Su and Li [12] by adopting a factor of six, value selected specifically to validate the double hardening bounding surface sand model [18–20] used in the computer program SUMDES [17]. Following the aforementioned procedure, an *agitation* factor of four was defined for the present study. Therefore, considering the laboratory hydraulic conductivity of Toyoura sand at 1 g of 2×10^{-4} m/s, and centrifuge and *agitation* scaling factors of 40 and 4, respectively, the hydraulic conductivity used in the prototype scale simulation was 3.2×10^{-2} m/s. Table 3 summarizes the material properties used for the corresponding simulations of the centrifuge tests on Toyoura sand.

Figs. 5–7 reveal SANISAND performance when predicting the volumetric response of the centrifuge tests in terms of Δu and surface settlement during BD shearing. Fig. 5 depicts the r_u time-histories during shaking resulting from motions 1 and 2 at depths of 6 and 12 m. It can be seen that the simulations capture both the peak values of r_u and its rate of increase reasonably well under both base motions and at both monitored depths. Some discrepancies between the experiments
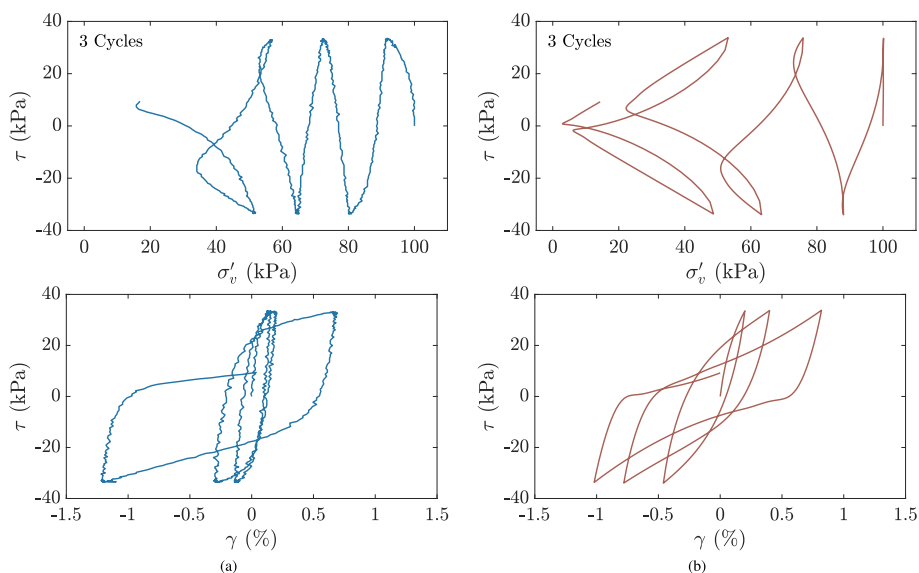
Fig. 4. Response of Toyoura sand with $D_r = 55\%$ in undrained cyclic torsional tests: (a) experiment [52] and (b) simulation.

and simulations can be observed as excess pore water pressure starts to dissipate; this phase of response is controlled largely by the hydraulic conductivity of soil. Also, the simulations show signs of dilation spikes while the experiment show a rather smooth variations in the r_u time histories. Fig. 6 summarizes the depth profiles of Δu_{peak} achieved during testing and simulations. The numerical results capture to a reasonable degree the trend and magnitude of the experimental evidence for both motions, showing the model is sensible to changes in shearing amplitude for elements at different initial confining pressures. Fig. 7 shows a good fit between the observed and simulated surface settlement time-histories during the application of shearing, where both the rate and the maximum of settlement were replicated. The experimental results suggest that most of the settlement occurred during shaking, which is typically the case for relatively permeable homogenous deposits with no surface crust. These settlements were mostly caused by partial drainage and excess pore water pressure dissipation during to shaking,

which indicates that the numerical model is able to capture these mechanisms of volumetric response. Note that Su and Li [12] reported the surface settlement time-history for motion 1, while Su et al. [48] only provided the maximum surface settlement for motion 2; in both cases the settlements were reported only until the application of the shaking phase. Finally, Fig. 8 presents a comparison of the recorded and simulated acceleration time-histories in the x direction at the depth of 8 m. The comparison for motion 1, which at 8 m did not induce very high values of r_u (see Figs. 5a and 6a), shows a good agreement between the simulation and experiment. For motion 2 with the much stronger shaking, the simulated accelerations shows moderate dilation spikes in 10–16 s, presumably due to variations stiffness between the contractive and dilative phases of response where the stress path crosses the dilatancy surface. The recorded acceleration response, including the dilation spikes, support the simulated values until around 12 s, but not beyond that. Beyond this point, the level of propagated acceleration in

Table 3
Numerical and constitutive model parameters for the soil columns used in the simulations.

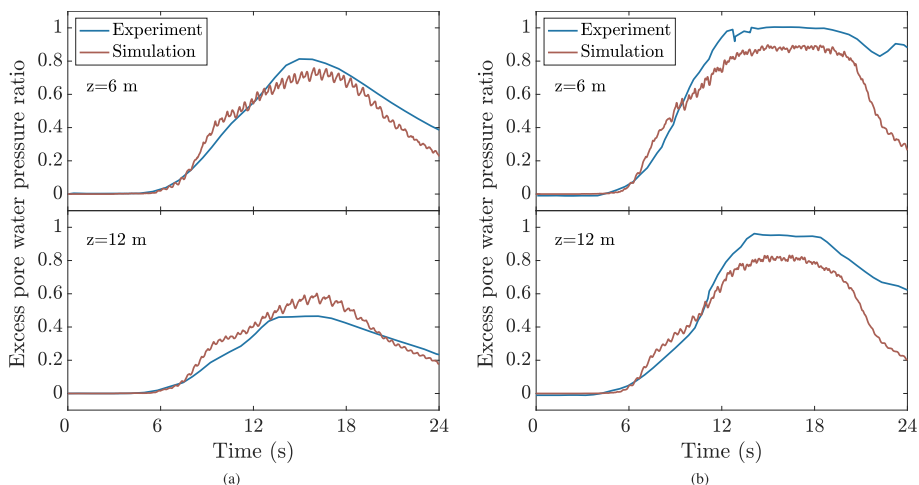| Description	Parameter	Symbol	Toyoura sand	Nevada sand	Monterey sand
General properties	Solid density (kg/m³)	ρ_s	1420	1650	1835
	Initial void ratio	e	0.825	0.60, 0.66	0.78, 0.70, 0.61
	Hydraulic conductivity (m/s)	k	3.2×10^{-2}	2.2×10^{-5}	5×10^{-4}
Rayleigh damping	Minimum damping (%)	ξ_{min}	0.745	0.745	0.745
	Central frequency (Hz)	f_{min}	13.58	5.24	3.73
Isotropic fluid flow model	Fluid density (kg/m³)	ρ_f	1000	1000	1000
	Fluid bulk modulus (kN/m²)	K_f	2.2×10^6	2.2×10^6	2.2×10^6
SANISAND model	Elasticity	G_0	125	150	216
		ν	0.05	0.05	0.039
	CSL	M	1.25	1.14	1.32
		c	0.721	0.78	0.718
		e_0	0.934	0.83	0.849
		λ	0.019	0.027	0.01
		ξ	0.7	0.45	0.7
	Yield surface	m	0.02	0.02	0.03
	Plastic modulus	n^b	1.25	1.23	2.5
		h_0	7.05	9.7	7.93
		c_h	0.968	1.02	1.14
	Dilatancy	n^d	2.1	0.55	2.0
		A_0	0.704	0.1	0.213
	Fabric dilatancy	z_{max}	10	100	25
		c_z	1000	2000	1000
	Overshooting correction	$\bar{e}_{eq}^p$	0.01%	0.01%	0.01%
		n	1	1	1

Fig. 5. Excess pore water pressure ratio (r_u) time-histories at different depths in BD shearing centrifuge tests on Toyoura sand with $D_r = 40\%$ [48]: (a) motion 1 and (b) motion 2.
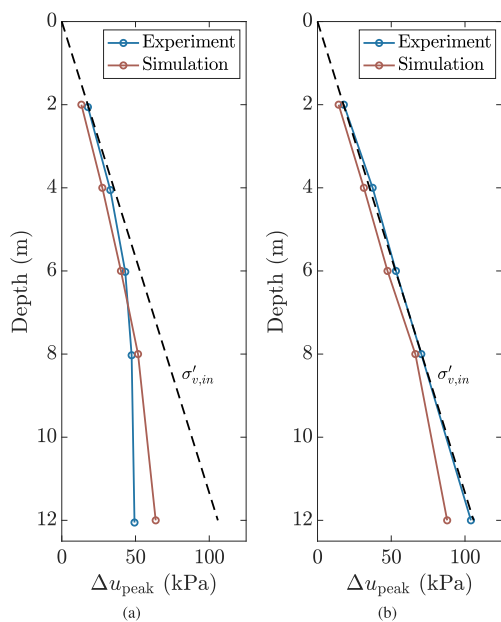

Fig. 6. Peak excess pore water pressure (Δu_{peak}) profiles in BD shearing centrifuge tests on Toyoura sand with $D_r = 40\%$ [48]: (a) motion 1 and (b) motion 2.

the experiment is less than the one simulated by the model. This perhaps can be explained from Figs. 5b and 6b which suggest that while in the experiment the entire soil column was liquefied, the base layers did not entirely liquefy in the simulation. Despite of this last observation, the simulations appear to reasonably capture the volumetric response of the soil deposit under this rather complex bidirectional shaking.
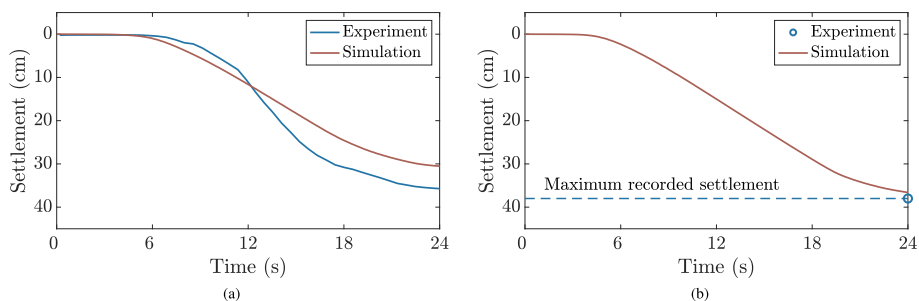
3.2. Bidirectional shaking of Nevada sand

3.2.1. Description of the centrifuge tests

El Shafee et al. [13,14] conducted BD shearing centrifuge tests in the Rensselaer Polytechnic Institute (RPI) Network for Earthquake Engineering Simulation (NEES) centrifuge facility by using a two-dimensional shaker to study the response of level ground saturated sand deposits. The tested models consisted of saturated uniform Nevada sand deposits with a thickness of 7 m. The soil deposits were prepared by dry pluviation without any tamping to achieve initial D_r of 45% and 75%, and were saturated using a fluid 25 times more viscous than water. The centrifuge tests made use of a laminar box consisting of dodecagonal rings stacked over each other. A detailed description of the testing procedure and instrumentation is given by El Shafee [59].

The results from two centrifuge tests were selected for validation, one for each level of D_r. Both of these tests were subjected to the same base excitation, which consisted of a BD synthetic shear pattern labeled here as motion 3, as listed in Table 2 and illustrated in Fig. 9. This motion had peak accelerations of 0.10 g in each direction, with dominant frequencies of 1, 2 and 3 Hz, and was generated by varying the phase angle between its orthogonal components in order to simulate a phase angle-time history similar to those of real earthquakes [13]. Results in terms of r_u and settlement time-histories at different depths were used for the validation purpose here.

3.2.2. Numerical simulations

The simulations for these tests made use of a 7 m-deep 3D soil column. SANISAND parameters considered the calibration for Nevada sand by Taiebat et al. [44] based on the constant-p monotonic and undrained cyclic triaxial tests reported by Arulmoli et al. [60]. Considering the very likely differences in cyclic response between the sand batch tested by Arulmoli et al. [60] ($D_{50} = 0.165$ mm, $e_{max} = 0.887$ and
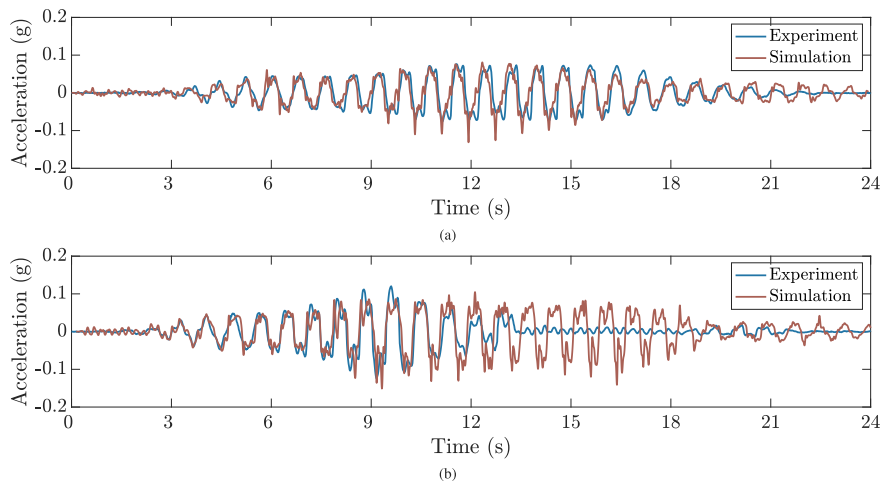

Fig. 7. Surface settlement time-histories in BD shearing centrifuge tests on Toyoura sand with $D_r = 40\%$ [12,48]: (a) motion 1 and (b) motion 2.

Fig. 8. Acceleration time-histories for the *x* direction at a depth of 8 m in BD shearing centrifuge tests on Toyoura sand with D_r = 40% [48]: (a) motion 1 and (b) motion 2.
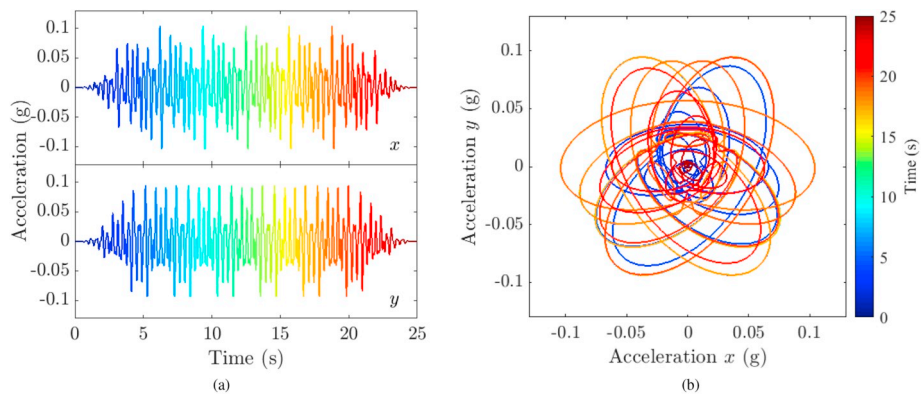

Fig. 9. Target horizontal (a) acceleration time-histories and (b) acceleration orbit of motion 1 as described by El Shafee et al. [13,14] used in BD shearing centrifuge tests on Nevada sand.

e_{min}= 0.511) and the batch used by El Shafee et al. [13,14] (D_{50} = 0.150 mm, e_{max}= 0.751 and e_{min}= 0.55), cyclic simple shear tests recently conducted by Kwan et al. [61] on Nevada sand ($D_{50} \approx 0.175$ mm, e_{max}= 0.76 and e_{min}= 0.56) were used to update the model calibration. The update focused on the parameters controlling the volumetric hardening and fabric dilatancy, and the calibrated parameters are summarized in Table 3. Fig. 10 shows the model performance in capturing the experimental results of a cyclic simple shear test up until the effective
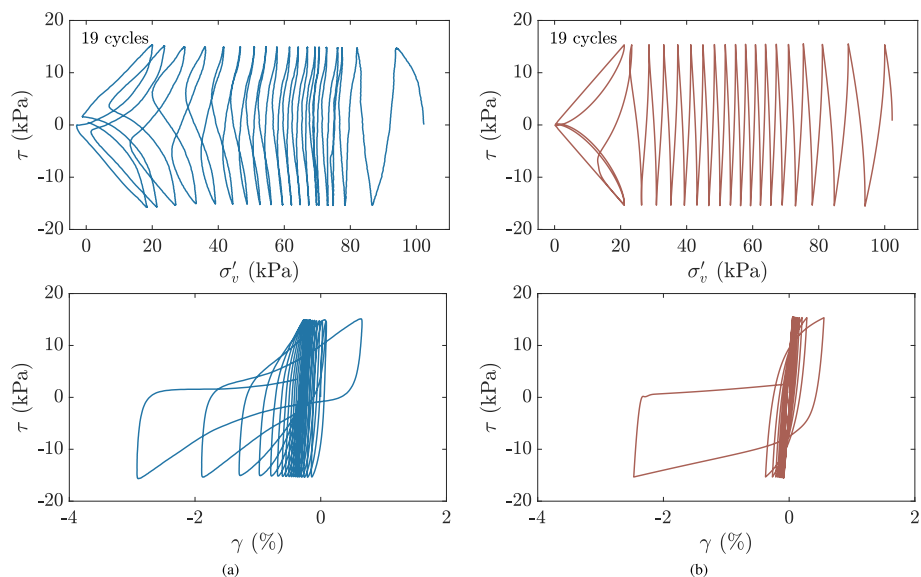

Fig. 10. Response of Nevada 120 sand with D_r = 45% in undrained cyclic simple shear tests: (a) experiment [61] and (b) simulation.
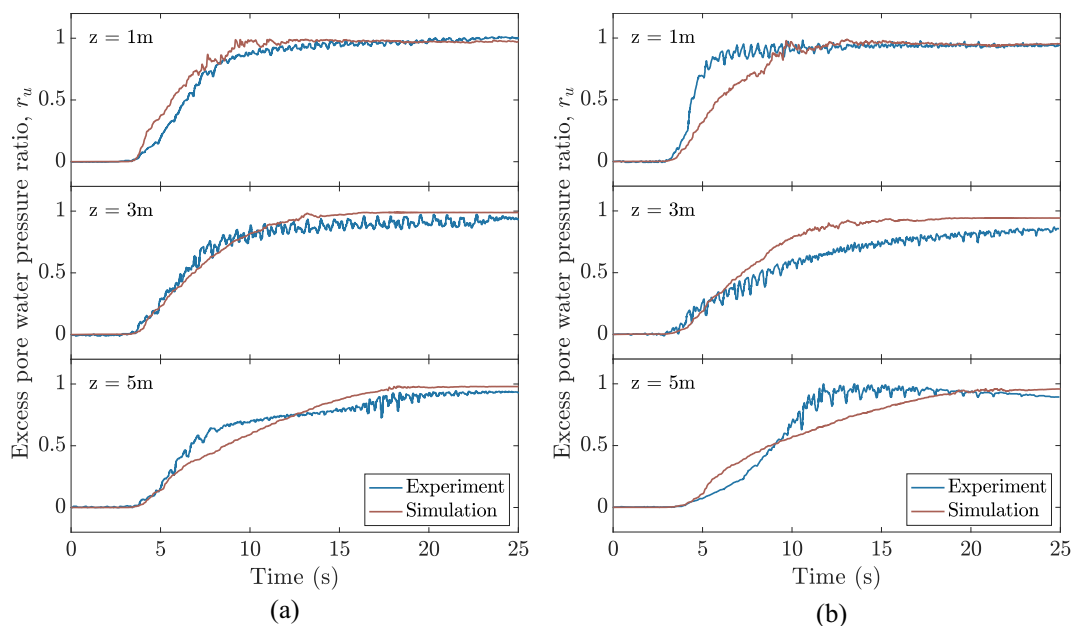
Fig. 11. Excess pore water pressure ratio (r_u) time-histories at different depths in BD shearing centrifuge tests on Nevada sand with: (a) D_r = 45% [13] and (b) D_r = 75% [14].

vertical stress reaches the onset of liquefaction. With no further adjustment, these calibrated model parameters were used to simulate the centrifuge tests. The hydraulic conductivity of 2.2×10^{-5} m/s reported in El Shafee et al. [13,14] was used for the simulations since the testing program used a high viscosity fluid consistent with the centrifuge scaling factor. The authors are not aware of reports on the phenomenon of *agitation* when this type of fluid with *g*-consistent viscosity is employed.

Fig. 11 compares the experimental and simulated r_u response for the BD shearing centrifuge tests with D_r = 45% and 75%, at depths of 1, 3, and 5 m. The results reveal that both centrifuge tests reached a state of liquefaction ($r_u \approx 1$) along almost all of their depth, without noticeable dissipation of excess pore water pressure during shaking. Fig. 11a for reveals that for D_r = 45% the model captured the overall r_u response at all control points, particularly for the $r_{u,peak}$, but without showing the apparent dilation spikes as seen in the experiment. For the denser test, depicted in Fig. 11b, the simulated rate of rise of r_u has more consistency with the experimental results at depth of 3 m and lesser consistency at depths of 1 and 5 m. Despite the mentioned discrepancies,

the numerical simulations and in particular the constitutive model appear capable of reasonably capturing the peak values of r_u achieved at the control points for both centrifuges, showing the sensibility of the model for prediction of $r_{u,peak}$ for different levels of D_r and confining pressures. Zeghal et al. [62] showed that the maximum surface settlements obtained during shaking for these experiments were between 1.6 cm and 2.5 cm, i.e. around 0.3% of the depth of the tested deposit. These values are significantly smaller than the settlements of 35–40 cm obtained in the Toyoura sand experiments (i.e., around 2% of the depth of the testes deposit). The negligible settlements during the shaking stage of the Nevada sand tests is a reflection of the relatively low level of permeability of this deposit compared to that of the Toyoura sand –see Table 3–, which caused a closed to undrained condition during the application of shearing to Nevada sand deposit. Consequently, it can be considered that almost all of the volumetric response of the deposit in the Nevada sand tests were manifested as excess pore water pressure. The numerical simulations reflected this observation, as the maximum settlements obtained were less than 1 cm. Finally, Fig. 12 compares the experimental and simulated acceleration time-histories in the *x*
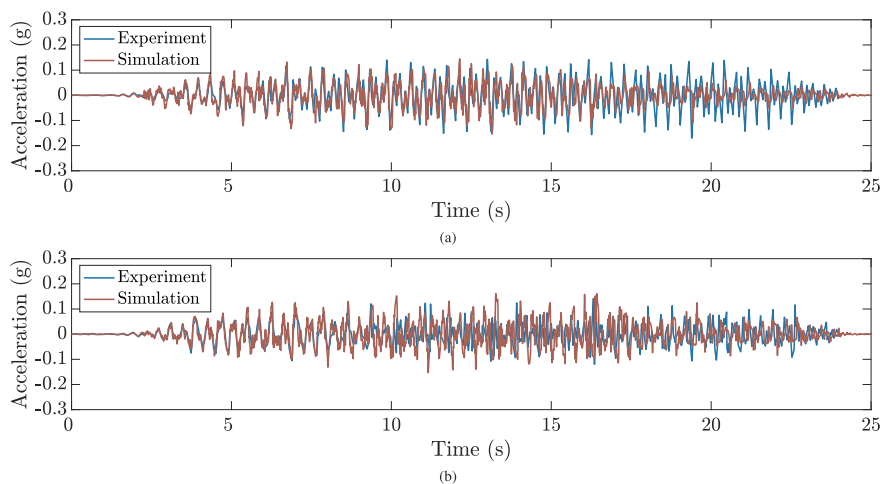

Fig. 12. Acceleration time-histories for the *x* direction at a depth of 5 m in BD shearing centrifuge tests on Nevada sand with: (a) D_r = 45% [13] and (b) D_r = 75% [14].

direction at depth of 5 m for both deposits. Fig. 12a shows that the model matches reasonably well the acceleration response for test with $D_r = 45\%$ until the soil approached a r_u close to 1 at around 16–17 s. At this point, the experiments showed dilation spikes both in the acceleration and excess pore water pressure response (see also Fig. 11a), but the simulations appear to not show those spikes as strongly as the experiments. Similarly, Fig. 12b shows that experiments and simulation match up until 9–10 s, but show differences beyond that time which might arise from the fact that the r_u rose faster in the experiment than in the simulations.

As discussed earlier, the model has some shortcomings in capturing the deviatoric response at the liquefaction state, which would influence the accelerations beyond the onset of liquefaction. The simulations in this section however provide some evidences that these shortcomings do not prevent the model from successfully capturing the overall r_u and settlement response during the shaking process. In combination with similar findings for numerical predictions of centrifuge tests under UD shearing reported by Tasiopoulou et al. [45] and Ramirez et al. [40] for the same constitutive model, it appears that SANISAND model can provide a reasonable estimate of the shear-induced volumetric response of level ground sand deposits during shaking for several scenarios including different intensities of the base input motions, a number of shearing patterns in UD and BD shaking, and a range of soil D_r. These were possible by using a single set of model parameters per sand, determined using conventional UD laboratory shear tests. Moreover, the successful simulations were achieved in spite of factors involved in centrifuge testing that were not considered in the analyses such as modeling the change of hydraulic conductivity during shaking and considering lateral pore water pressure dissipation, which are likely to have contributed in the mismatches observed for rate of generation of Δu.

4. The increase of volumetric response

Relying on the capability of the model in capturing the shear induced volumetric response of sands in bidirectional shaking, this section presents a series of numerical analyses conducted to quantify the impact of BD seismic shaking on dry and saturated level ground sand deposits. The numerical analyses focused on the following engineering demand parameters (EDP): surface settlement for dry deposits, and excess pore water pressure response during shaking for fully saturated deposits. Detailed description of the numerical model configuration, soil properties, and selected ground motions are presented below.

4.1. Numerical models and selection of ground motions

The numerical simulations conducted involved modeling the response of a 30 m-deep sand deposit overlying a rigid and impermeable bedrock. Two different types of scenarios were simulated: a dry sand deposit configured without any pore water and a saturated sand deposit with water table at the ground surface and allowing only vertical flow of the pore water. For both of these models, three different levels of $D_r = 30$, 55 and 80% were considered. These values aimed to represent uniform single-layered deposits of loose, medium dense and dense sand, respectively. As in the validation exercise, the numerical analysis database was built using $FLAC^{3D}$. The simulations considered dry and fully water-saturated soil columns with a height of 30 m, spatially discretized with 60 cubic brick zones with a Δh of $0.5 \times 0.5 \times 0.5$ m and with a Δt of 10^{-5} s. The base of the model was set as rigid while the side nodes were horizontally tied at each elevation to ensure 1D wave propagation, hence being consistent with the numerical configuration adopted in the validation section. Similarly, the dynamic stage considered Rayleigh damping with a target value of 1% was used. Surface settlements were monitored during the application of the motion in dry models. For the saturated cases, water flow was modeled using the built-in isotropic fluid flow model of the program, allowing to record
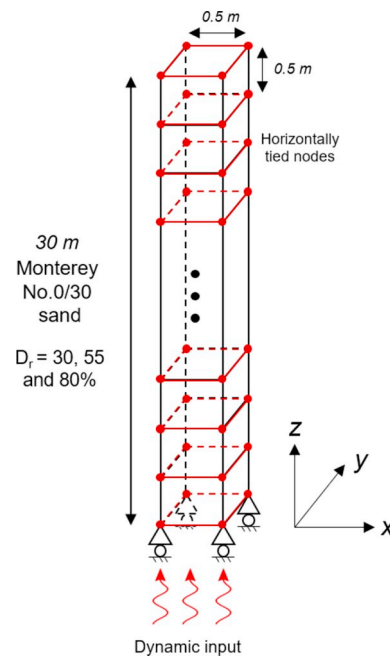

Fig. 13. Numerical configuration of soil column model used for the simulations.

the pore water pressures in every 2 m along the height of the column. A constant and isotropic hydraulic conductivity $k = 5 \times 10^{-4}$ m/s was chosen for the analyses; this is the average of the k values used for the simulations of the centrifuge tests in the validation section. The selected hydraulic conductivity resulted in an almost undrained condition during shaking, thus preventing the shear-induced volumetric response of the model to partly exhibit in form surface settlement due to partial drainage and/or pore water pressure dissipation. Fig. 13 shows details of the model set up.

The SANISAND parameters adopted for the analyses were those calibrated by Yang et al. [31] for Monterey No. 0/30. This set of parameters was chosen as they were evaluated against BD cyclic shear tests, therefore allowing for a direct element to boundary value scale comparison. In the present study, the shear modulus parameter G_0 was increased to represent a soil column with an initial V_{s30} of around 200 m/s. This increase also reflects the fact that the original value of G_0 for Monterey No. 0/30 sand in the SANISAND formulation was calibrated from monotonic triaxial tests, which can lead to an underestimation of the soil deposit stiffness [63]. Table 3 presents details of the numerical and constitutive model properties of the soil column.

The models analyzed were subjected to a series of 40 pairs of non-scaled shallow crustal earthquake ground motions obtained from the PEER Strong Motion Database [64] for stations at site classes C and D according to the NEHRP V_{s30} classification [65]. These recordings were selected to cover a considerable range of source parameters: earthquake Moment magnitude (M_w) ranging from 5.8 to 7.6 and rupture distance (R_{rup}) from 16 to 88 km. Additionally, they were chosen in order to cover a wide range of earthquake intensity measures (IMs), particularly those that have been historically used in liquefaction triggering analysis, such as peak ground acceleration (PGA) and Arias intensity (I_a) [66,67], and more recent ones associated with excess pore water pressure response such as Cumulative Absolute Velocity after application of 5 cm/s² as threshold acceleration or CAV_5 [68]. The selected earthquakes and their main characteristics are summarized in Table 4. Also, Fig. 14 illustrates their source parameter distribution. Ground motions recorded at sites with R_{rup} smaller than 16 km were intentionally avoided to prevent dealing with the effect of forward directivity. This was checked by selecting ground motions whose x and y components exhibited similar values of IMs, such as I_a. Therefore, the motions chosen in this study are expected to not have any directivity or

Table 4
Ground motions used for the simulations of the non-scaled dataset.

No.	Earthquake	Year	Station	M_w	R_{rup}	V_{s30}	PGA (g)		I_a (m/s)		CAV_5 (m/s)	
							x	y	x	y	x	y
1	Chi-Chi Taiwan	1999	CHY014	7.6	34.18	348	0.26	0.23	1.63	1.62	14.37	14.17
2	Chi-Chi Taiwan	1999	CHY025	7.6	19.07	278	0.16	0.14	1.17	0.96	14.65	13.45
3	Chi-Chi Taiwan	1999	CHY065	7.6	83.43	250	0.12	0.09	0.48	0.33	9.20	7.48
4	Imperial Valley-06	1979	CRP	6.5	15.19	472	0.15	0.17	1.27	1.15	15.18	13.43
5	Imperial Valley-06	1979	VCT	6.5	31.92	242	0.17	0.12	0.25	0.20	4.90	4.69
6	Joshua Tree	1992	TPP	6.1	17.86	334	0.20	0.19	0.61	0.51	6.28	5.50
7	Kobe	1995	KKG	6.9	22.50	312	0.33	0.25	1.61	0.98	11.13	8.91
8	Kobe	1995	SOK	6.9	19.15	256	0.23	0.21	0.79	0.61	6.74	6.48
9	Landers	1992	CWT	7.3	19.74	353	0.41	0.28	2.09	1.17	10.87	8.83
10	Landers	1992	MVF	7.3	17.36	396	0.23	0.14	1.16	0.69	12.59	10.41
11	Landers	1992	PSA	7.3	36.15	312	0.09	0.07	0.35	0.30	8.00	7.53
12	Loma Prieta	1989	HVY	6.9	30.49	282	0.13	0.10	0.25	0.24	4.65	4.23
13	Loma Prieta	1989	PAS	6.9	30.86	425	0.26	0.20	0.88	0.54	7.55	6.10
14	Loma Prieta	1989	SJW	6.9	32.78	280	0.11	0.08	0.23	0.15	4.45	3.92
15	Morgan Hill	1984	CPT	6.2	39.08	289	0.13	0.10	0.22	0.15	3.42	3.06
16	N. Palm Springs	1986	ICC	6.1	41.93	339	0.23	0.24	0.34	0.32	3.80	3.68
17	N. Palm Springs	1986	SJS	6.1	23.31	447	0.05	0.05	0.05	0.05	1.79	1.76
18	Northern Calif-05	1954	FCH	6.5	27.02	219	0.17	0.20	0.53	0.36	6.45	5.16
19	Northridge-01	1994	BHM125	6.7	18.36	546	0.61	0.43	2.89	2.26	11.63	10.62
20	Northridge-01	1994	BHM141	6.7	17.15	356	0.14	0.09	0.27	0.18	4.27	3.72
21	Northridge-01	1994	CORR	6.7	20.72	450	0.17	0.13	0.31	0.18	4.19	3.30
22	Northridge-01	1994	GLP	6.7	22.21	371	0.26	0.19	0.71	0.50	5.86	5.06
23	Northridge-01	1994	LPS	6.7	31.33	305	0.48	0.42	4.33	2.96	15.46	13.84
24	Northridge-01	1994	LCN	6.7	18.50	412	0.46	0.60	3.01	2.62	14.29	12.48
25	Northridge-01	1994	LOA	6.7	39.91	312	0.36	0.20	1.13	0.58	7.77	6.12
26	Northridge-01	1994	LV2	6.7	37.24	436	0.18	0.10	0.25	0.18	4.10	3.80
27	Northridge-01	1994	LV4	6.7	37.57	421	0.21	0.17	0.43	0.28	4.66	3.85
28	Northridge-01	1994	LV5	6.7	37.80	375	0.15	0.08	0.22	0.18	4.66	4.38
29	Northridge-01	1994	LV6	6.7	38.03	327	0.09	0.07	0.07	0.06	2.02	1.67
30	Northridge-01	1994	PNS	6.7	36.12	397	0.08	0.06	0.10	0.08	2.45	2.32
31	Northwest China-04	1997	JSH	5.8	27.86	240	0.22	0.18	0.34	0.23	3.77	3.18
32	San Fernando	1971	LAH	6.6	22.77	316	0.20	0.17	0.64	0.42	6.50	5.38
33	San Fernando	1971	WND	6.6	39.45	299	0.10	0.10	0.17	0.12	3.61	2.75
34	Superstition Hills-02	1987	ECI	6.5	18.20	192	0.37	0.29	1.06	0.71	10.67	9.90
35	Taiwan SMART1	1986	SMR	7.3	53.31	308	0.18	0.14	0.69	0.65	8.41	8.84
36	Umbria Marche	1997	GPN	6.0	35.91	492	0.10	0.10	0.24	0.22	5.20	5.18
37	Whittier Narrows-01	1987	BNB	6.0	26.34	321	0.17	0.21	0.37	0.33	4.26	4.10
38	Whittier Narrows-01	1987	HBL	6.0	44.58	316	0.04	0.04	0.03	0.02	1.09	1.14
39	Whittier Narrows-01	1987	IUO	6.0	25.86	316	0.26	0.20	0.48	0.32	4.25	3.85
40	Whittier Narrows-01	1987	NSS	6.0	41.69	281	0.15	0.12	0.23	0.16	3.93	3.55
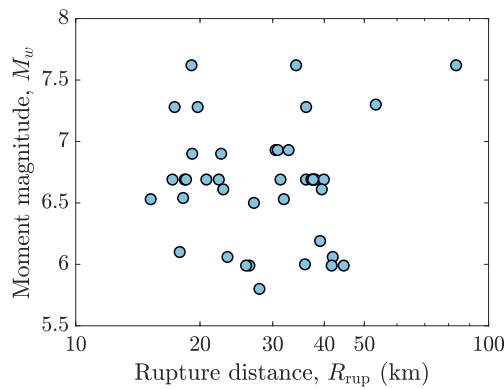
Fig. 14. Earthquake source parameter distribution in terms of Moment magnitude and rupture distance.

Fig. 15. Time-histories of I_a and CAV_5 of the horizontal components from the 1995 Kobe earthquake at the Shin-Osaka station (calculated from data of PEER Strong Motion Database [64]).

dominant direction, as suggested in the acceleration orbit in Fig. 1. Following this criterion, the analyses focused on understanding the effects BD loading without considering the orientation of the numerical model with respect to the ground motion direction. Fig. 15 illustrates the time-histories of I_a and CAV_5 of the 1995 Kobe Earthquake recorded at the Shin-Osaka station. Nevertheless, for the sake of consistency, the recording with the highest value of I_a between the pair of horizontal components per ground motion was the one applied in the x direction in
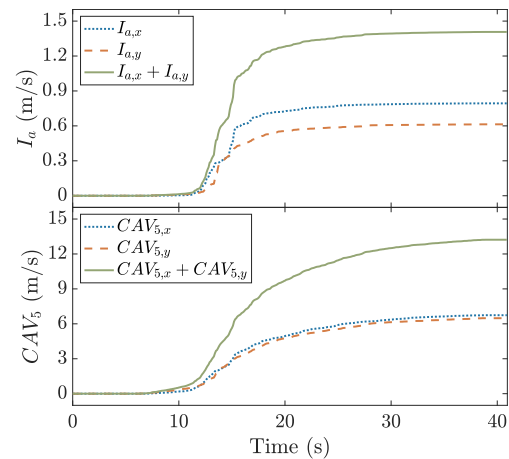
the numerical model. Finally, the seismic records were not deconvoluted nor modified to consider the stiffnesses of the recording sites and of the rigid bedrock since the intent of this study is to merely gain insight about the comparative response of the deposits in UD and BD seismic shearing.

Table 5
Summary of numerical models evaluated for the non-scaled dataset.

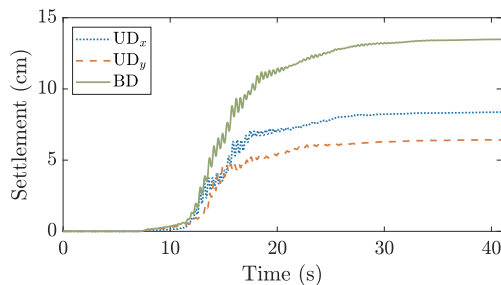| Description	Scenarios
Saturation condition	Dry and saturated
Relative density, D_r	30%, 55%, 80%
Loading case	UD_x, UD_y, BD
Number of earthquakes	40
Total number of simulations	**720**

Fig. 16. Settlement time-histories for UD and BD shearing computed for dry model with $D_r = 55\%$ subjected to ground motion No. 8.

The 40 selected ground motions (80 recordings in total considering the horizontal *x* and *y* components of each motion) were applied at the base of the model as acceleration time-histories to replicate cases of UD and BD seismic shearing. The excitations were applied separately in the *x* and *y* directions for UD shearing, and simultaneously in both directions for the BD shearing cases. Table 5 summarizes the analysis information related to the 2 (saturation conditions) × 3 (relative densities) × 3 (loading directions) × 40 (pairs of ground motions) = 720 cases evaluated.

4.2. Effect on settlement of dry deposits

The EDP considered for the dry models was surface settlement, obtained by recording the vertical displacement at the top of the soil column. Fig. 16 shows the computed surface settlement time-histories obtained from the analyses of the soil column with $D_r = 55\%$ when subjected to motion No. 8, according to Table 4. The results from the two UD analyses (UD_x and UD_y) resemble each other since, as intended, the ground motion has no dominant direction. However, there is a significant difference between the settlement results from the BD and UD shearing analyses; the settlement in the former developed at a faster rate and to a higher final magnitude. The accumulation of settlement for all scenarios followed the shape of the time-history of I_a, CAV_5, show in Fig. 15 for motion No. 8, and/or other evolutionary intensity measures. At the end of the earthquake excitations, the computed
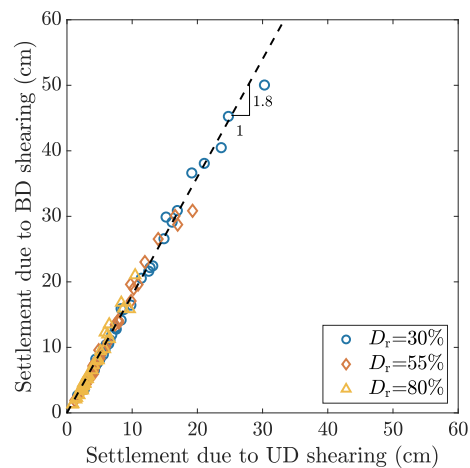

Fig. 18. Comparison of settlements obtained from the UD and BD shearing analyses of the dry model.

settlement under the BD shearing is nearly 80% higher than those under the corresponding UD shearing. To further look into the extent of these differences, Fig. 17 presents contours of settlement for the same motion at different depths, and for the UD_x and BD shearing cases. By focusing on the settlement contour of 5 cm, the results exposed how BD shearing not only increased the rate of settlement development along the depth of soil column, but also induced this level of settlement at around a depth of 18 m compared to the 12 m for the UD_x shearing case.

Fig. 18 summarizes the surface settlement results from all the analyses performed for the dry model. Each point in this plot represents the results related to one of the 40 pairs of ground motions and one of the three D_r. The horizontal axis shows the mean surface settlement from the UD_x and UD_y analyses, while the vertical axis shows the surface settlement from the BD analysis. In all cases, the magnitude of settlement was obtained at the end of seismic excitation. The results show that the highest settlements both for UD and BD shearing are observed for the soil column configuration with $D_r = 30\%$. The overall results indicate a uniform increase of 80% in surface settlement due to BD shearing. This increase does not appear to be significantly influenced by the level of D_r. While this latter observation differs with the findings of Bhaumik et al. [11] and Nie et al. [16], the increase percentage falls within the range of 50%–200% determined in their element-scale studies and resembles the 100% increase observed by Pyke et al. [1] in their shake table tests. Nevertheless, recent experimental and numerical observations determined in Bhaumik et al. [69] and in Ramirez et al. [40] suggest that assessing the seismic response of large-scale sand systems based only on one type of element-level tests may lead to comparison inconsistencies similar to those observed here.
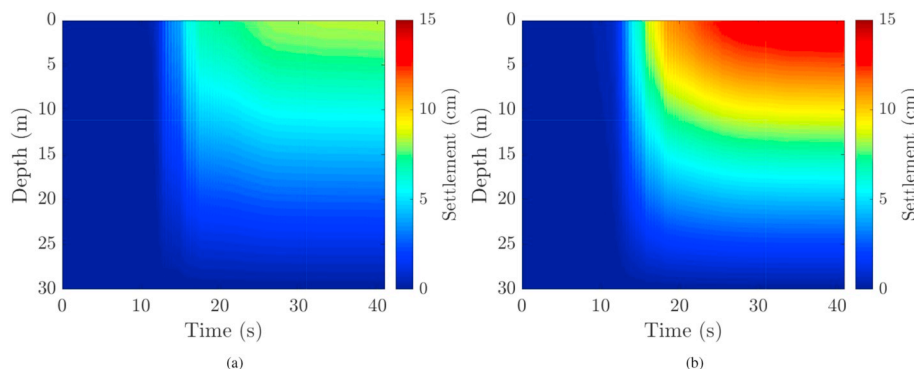

Fig. 17. Contours of settlement for (a) UD_x and (b) BD shearing computed for dry model with $D_r = 55\%$ subjected to ground motion No. 8.
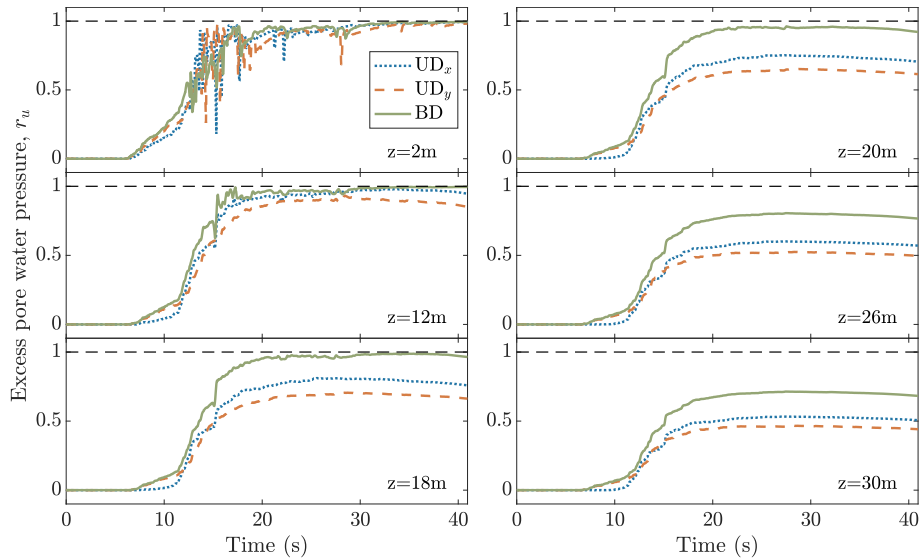
Fig. 19. Excess pore water pressure ratio (r_u) time-histories at different depths for UD and BD shearing computed for saturated model with $D_r = 55\%$ subjected to ground motion No. 8.

4.3. Effect on excess pore water pressure of saturated deposits

For the saturated cases, the excess pore water pressure response was chosen as EDP to obtain a scalar index for liquefaction hazard evaluation for both UD and BD shaking scenarios. The excess pore water pressure was monitored at every 2 m along the height of the soil column model and only during the application of the seismic shearing. Fig. 19 shows the excess pore water pressure ratio (r_u) time-histories developed during the analysis of a soil column with $D_r = 55\%$ when subjected to motion No. 8. In this study, the definition of r_u is taken as the ratio between excess pore water pressure and initial vertical effective stress. As in the dry models, the development of shear-induced volumetric response during shaking, represented here by r_u, resembles the shape of the time-history of evolutionary intensity measures of motion No. 8 as presented in Fig. 15. It can also be observed that the response of the UD_x and UD_y cases are similar to each other, and in general they are lower or equal to the BD case. The differences between the response at each depth during the UD and BD shearing regimes increase as peak r_u approaches the attractor value of 1 and decreases once peak r_u during BD shearing reaches its limit. Fig. 19 also shows that the r_u response near the surface exhibits higher dilation spikes during UD shearing than during BD shearing. This dilative behavior can be attributed to the fact that in the UD analyses the shear strain accumulates in one direction while in the BD case such strain is distributed on a horizontal plane, constantly changing the shearing direction, thus allowing for a smoother transition between loading and unloading. Conversely, in UD
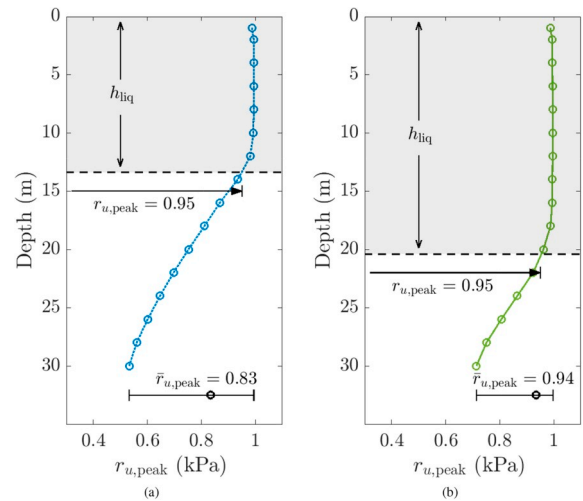

Fig. 21. Profiles of maximum excess pore water pressure ratio ($r_{u,\text{peak}}$) for (a) UD_x and (b) BD shearing computed for saturated model with $D_r = 55\%$ subjected to ground motion No. 8.

shearing the strains are concentrated in one direction and abruptly change in the opposite direction upon unloading. Similar observations regarding the differences in dilation spikes were noticed by El Shafee
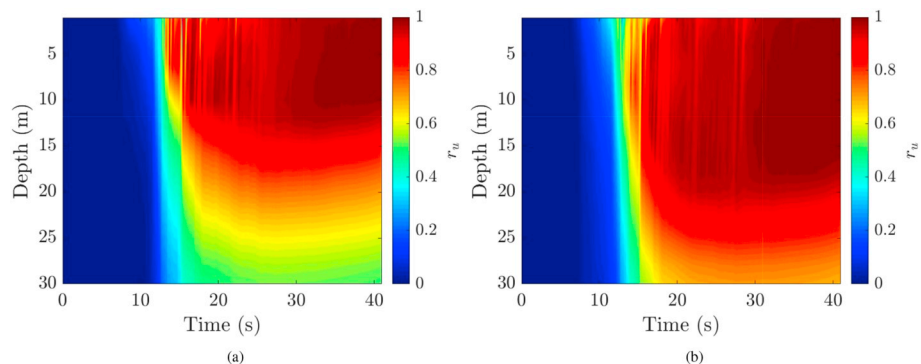

Fig. 20. Contours of excess pore water pressure ratio (r_u) for (a) UD_x and (b) BD shearing computed for saturated model with $D_r = 55\%$ subjected to ground motion No. 8.
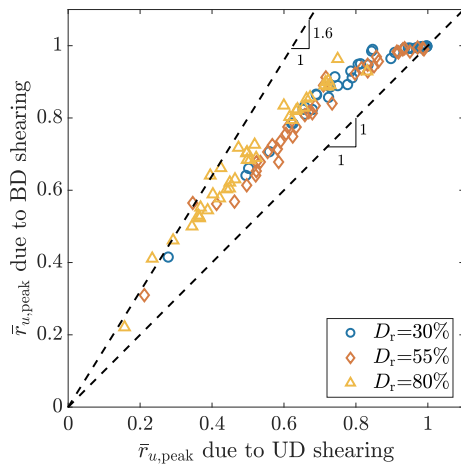
Fig. 22. Comparison of the mean of maximum excess pore water pressure ratio $\bar{r}_{u,\text{peak}}$ obtained from the UD and BD shearing analyses of the saturated model.

et al. [13] through their centrifuge tests.

Fig. 20 shows the contours of r_u for the same motion at different depths and times for the UD_x and BD analyses. These results indicate that excess pore water pressure at different elevations started to rise at between 8 s and 11 s and reached their peak values ($r_{u,\text{peak}}$) at 30 s for the UD_x case and at 20 s for the BD analysis, showcasing a faster increase of excess pore water pressure during the latter. Both Figs. 19 and 20 also show that the thickness of the layer reaching or exceeding an $r_{u,\text{peak}}$ value between 0.85 and 1.0 is greater during BD loading than during UD loading. For more detail, Fig. 21 presents the profile of $r_{u,\text{peak}}$ for the same soil column. Here, h_{liq} is defined as the thickness of the layer exceeding an $r_{u,\text{peak}}$ value of 0.95 – a threshold chosen for illustrative purposes. It is shown then that $h_{\text{liq}} \approx 13$ and 20 m for the UD_x and BD analyses, respectively. Evidently, this increase of h_{liq} of 7 m caused by BD shearing is significant considering the depth of the soil column. The observations presented here in terms of increase of rate and magnitude of excess pore water pressure response and h_{liq} are similar to what was determined in previous in experimental and numerical studies for relatively large-scale saturated systems [e.g., 12–14, 21] and are conceptually similar to what was determined for the dry models in an earlier section.

To further expand on the comparison, an additional index of performance, labeled as $\bar{r}_{u,\text{peak}}$, was proposed based on the depth-average of the $r_{u,\text{peak}}$ profile. More specifically and as shown in Fig. 21, the $\bar{r}_{u,\text{peak}}$ for an analysis is the average of the $r_{u,\text{peak}}$ values obtained at different control points along the soil deposit. The $\bar{r}_{u,\text{peak}}$ reasonably captures the
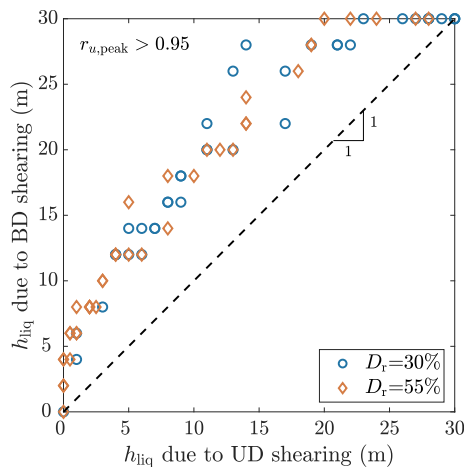

Fig. 23. Comparison of the thickness of the layer with $r_{u,\text{peak}} > 0.95$ due to BD shearing in 30 m-deep sand deposits with $D_r = 30\%$ and 55%.
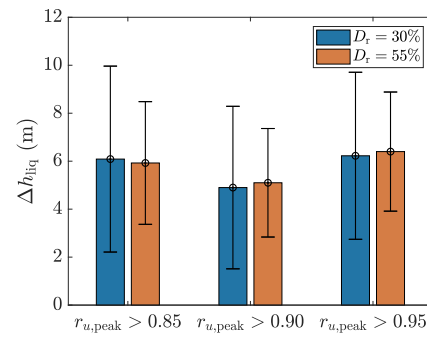

Fig. 24. Mean and standard deviation of the increased thickness of the layer with $r_{u,\text{peak}}$ exceeding different thresholds (0.85, 0.90, and 0.95) due to BD shearing in 30 m-deep sand deposits with $D_r = 30\%$ and 55%.

overall developed excess pore water pressure of each model, and allows to more readily summarize the results from all the analyses. An $\bar{r}_{u,\text{peak}} = 1$ indicates that the entire deposit has reached the onset of liquefaction due to seismic shearing. A summary of $\bar{r}_{u,\text{peak}}$ is presented in Fig. 22, where the x axis represents the average response between the UD_x and UD_y analysis while the y axis shows the response for the BD case. In general, $\bar{r}_{u,\text{peak}}$ developed under the BD shearing was up to 60% higher than the values obtained in UD shearing. Naturally, this increase becomes smaller as $\bar{r}_{u,\text{peak}}$ approaches 1. Similar to previous findings [e.g., 12], the increase of $\bar{r}_{u,\text{peak}}$ in the loose sand case was observed to be generally smaller, at around 20%, since $\bar{r}_{u,\text{peak}}$ exhibited values close to 1 in both UD and BD loading analysis for the cases of moderate to strong earthquakes. Nevertheless, in dense sands, where the developed $\bar{r}_{u,\text{peak}}$ values are in general smaller than in the loose case, the increase can be as much as 60%, as can be deduced from the findings of Cerna-Diaz et al. [15].

Fig. 23 summarizes the developed h_{liq} for an $r_{u,\text{peak}} > 0.95$ in all the saturated analyses with $D_r = 30\%$ and 55%. For each earthquake scenario, the mean result for the UD analyses and the one for the corresponding BD analysis are presented in the x and y axes, respectively. The UD shearing developed small or even non-existent liquefied layer for the relatively *weak* earthquakes, resulting in h_{liq} values ranging from 0 to 5 m. For these same earthquakes, the BD shearing generated larger h_{liq} values of 0–10 m. For the scenarios where the h_{liq} for the UD shearing falls between 5 and 20 m, the increment of the liquefied layer thickness in the corresponding BD shearing became larger and more consistent, in the range of 5–10 m. For the *strongest* earthquakes, nearly the whole soil column was liquefied in both UD and BD shearing. The bidirectional shearing scenario leading to liquefaction of the entire soil column was observed in some of the centrifuge and numerical modeling cases presented earlier in Sec. 3.

To thoroughly address the increase of h_{liq} caused by BD shearing (Δh_{liq}), three different thresholds of $r_{u,\text{peak}}$ to define the h_{liq} were chosen: 0.85, 0.90 and 0.95. Using these values, Fig. 24 compiles the results from the simulations of the saturated model for $D_r = 30\%$ and 55% by showing the mean and standard deviation values of Δh_{liq}. It is shown that h_{liq} due to BD shearing can be in average between 5 and 6 m thicker for a 30 m-deep sand deposit, and it is not affected significantly by the selection of $r_{u,\text{peak}}$ threshold. The results for the dense case are not shown because for that case the $r_{u,\text{peak}}$ reaching values between from 0.85 to 1 might be indicator of the beginning of a progressive accumulation of shear strains, i.e., cyclic mobility, rather than of a sudden decrease of stiffness and strength, i.e., liquefaction.

5. Analysis considering a target seismic hazard

5.1. Numerical models and ground motion scaling

The implications of considering UD vs. BD seismic shearing can also

Table 6
Ground motions used for the simulations of the linearly scaled dataset.

No.	Earthquake	Year	Station	M_w	R_{rup}	V_{s30}	PGA (g)		I_a (m/s)		CAV_5 (m/s)	
							x	y	x	y	x	y
41	Borrego	1942	ELC009	6.5	56.9	213	0.07	0.05	0.09	0.06	3.29	2.73
42	Borrego Mtn	1968	ELC009	6.6	45.7	213	0.13	0.06	0.24	0.15	5.75	5.19
43	El Alamo	1956	ELC009	6.8	121.7	213	0.05	0.03	0.10	0.05	3.48	2.28
44	Friuli	1976	CDP	6.5	33.4	249	0.06	0.09	0.14	0.13	3.50	3.32
45	Friuli	1976	CNG	6.5	80.4	352	0.07	0.05	0.07	0.04	2.00	1.56
46	Imperial Valley-06	1979	CFS	6.5	24.6	206	0.13	0.08	0.15	0.10	3.63	3.05
47	Imperial Valley-06	1979	ELC013	6.5	22.0	250	0.11	0.07	0.18	0.11	3.86	3.33
48	Imperial Valley-06	1979	NFS	6.5	36.9	212	0.12	0.14	0.27	0.27	5.05	5.04
49	Irpinia	1980	RIV	6.9	30.1	575	0.10	0.10	0.35	0.31	6.55	6.13
50	Irpinia	1980	RIV	6.2	22.7	575	0.10	0.10	0.26	0.16	5.03	3.82
51	Kern County	1952	LAH	7.4	117.8	316	0.04	0.06	0.10	0.10	3.60	3.47
52	Kern County	1952	PCA	7.4	125.6	415	0.05	0.05	0.11	0.06	3.54	2.45
53	Kern County	1952	SBC	7.4	82.2	515	0.09	0.13	0.24	0.29	5.12	6.05
54	Northern Calif-02	1952	FCH	5.2	43.3	219	0.05	0.08	0.05	0.05	1.49	1.52
55	Northwest Calif-01	1938	FCH	5.5	53.6	219	0.15	0.09	0.10	0.08	1.93	1.75
56	San Fernando	1971	CCD	6.6	61.8	235	0.07	0.07	0.09	0.11	2.54	2.91
57	San Fernando	1971	LH1	6.6	27.4	425	0.15	0.11	0.26	0.20	4.11	4.10
58	Tabas	1978	BSH	7.4	28.8	325	0.11	0.08	0.27	0.26	4.94	4.98
59	Tabas	1978	FRS	7.4	91.1	303	0.09	0.10	0.19	0.21	4.41	4.90
60	Taiwan SMART1	1981	SMM001	5.9	27.4	268	0.18	0.08	0.23	0.09	2.92	2.26

be evaluated in analyses for a specified site seismic hazard. For this purpose, the development of settlement and excess pore water pressure response was evaluated for the target seismic hazard of a hypothetical site located in Seattle, WA, USA, which was first presented as an engineering application example in Kramer and Mitchell [68]. The simulations were completed for dry and saturated 30-m deep single-layered soil columns with a $D_r = 55\%$. A new suite of 20 *linearly scaled* ground motions, summarized in Table 6, was selected as shaking input considering the same criteria described in section 4.1. These motions were purposely not included in the database developed for the previous analyses to avoid any bias in the results of the exercise. Each horizontal acceleration time-history was scaled to meet the desired level of seismic hazard for the target site; the calculation of scaling factors (SFs) of each ground motion for the UD and BD shearing analyses followed this procedure:

- Target values of $PGA = 0.20$ g, $I_a = 0.23$ m/s and $CAV_5 = 3.15$ m/s were defined based on a probabilistic hazard analysis for the site in

Table 8
Summary of numerical models evaluated for the linearly scaled dataset.

Description	Scenarios
Saturation condition	Dry and saturated
Relative density, D_r	55%
Loading case	UD_x, UD_y, BD
Target intensity measure	PGA, I_a, CAV_5
Number of earthquakes	20
Total number of simulations	**360**

Seattle, and for a return-period of 100 years [68]. These values are representative of the same expected seismic hazard.

- The PGA, I_a and CAV_5 values for the non-scaled components of each ground motion were computed and reported in Table 6.
- To complete the UD shearing analyses, the x and y components of each ground motion were separately multiplied by their corresponding SFs so that each met the expected hazard. This process was
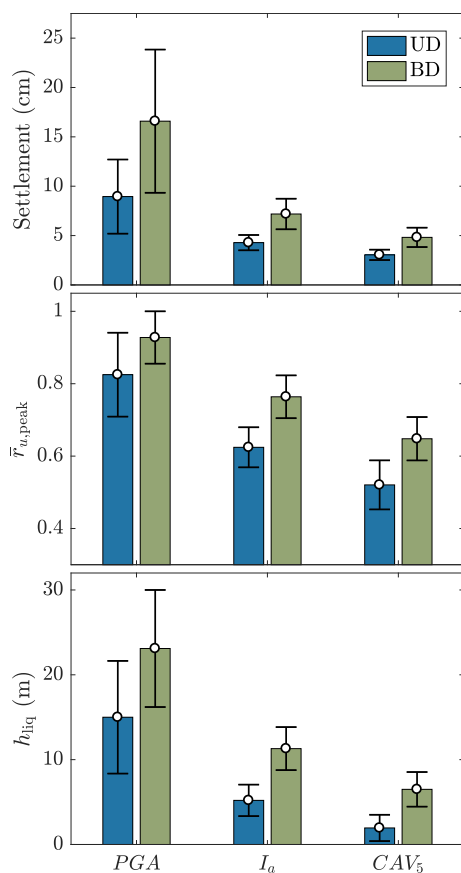
Table 7
Scaling factors used in the simulations of the linearly scaled dataset.

No.	Earthquake	Unidirectional shearing						Bidirectional shearing		
		$SF_{PGA,x}$	$SF_{PGA,y}$	$SF_{I_a,x}$	$SF_{I_a,y}$	$SF_{CAV_5,x}$	$SF_{CAV_5,y}$	SF_{PGA}	SF_{I_a}	SF_{CAV_5}
41	Borrego	3.03	4.41	1.59	1.88	0.97	1.10	2.29	1.10	0.66
42	Borrego Mtn	1.50	3.47	0.98	1.22	0.63	0.69	3.66	1.73	1.04
43	El Alamo	3.86	5.94	1.00	2.10	0.93	1.26	4.80	1.80	1.08
44	Friuli	3.23	2.19	1.29	1.32	0.92	0.96	2.67	1.31	0.94
45	Friuli	2.89	4.03	1.76	2.31	1.43	1.73	3.42	2.02	1.58
46	Imperial Valley-06	1.55	2.54	1.23	1.50	0.88	1.02	1.99	1.37	0.96
47	Imperial Valley-06	1.82	2.89	1.11	1.43	0.84	0.95	2.30	1.27	0.90
48	Imperial Valley-06	1.70	1.44	0.92	0.93	0.66	0.66	1.56	0.92	0.66
49	Irpinia	2.08	2.01	0.81	0.86	0.52	0.55	2.05	0.84	0.53
50	Irpinia	2.00	2.08	0.94	1.18	0.68	0.85	2.05	1.06	0.76
51	Kern County	4.73	3.38	1.50	1.50	0.90	0.93	4.01	1.51	0.92
52	Kern County	3.74	4.16	1.41	1.88	0.92	1.18	3.95	1.63	1.05
53	Kern County	2.23	1.51	0.98	0.89	0.69	0.60	1.84	0.94	0.64
54	Northern Calif-02	3.69	2.63	2.10	2.08	1.77	1.70	3.12	2.10	1.75
55	Northwest Calif-01	1.33	2.23	1.50	1.74	1.51	1.63	1.72	1.62	1.58
56	San Fernando	2.81	2.81	1.58	1.42	1.18	1.06	2.81	1.49	1.12
57	San Fernando	1.32	1.76	0.94	1.07	0.81	0.81	1.52	1.00	0.81
58	Tabas	1.89	2.35	0.90	0.92	0.65	0.65	2.11	0.93	0.65
59	Tabas	2.15	1.91	1.10	1.04	0.75	0.68	2.02	1.07	0.71
60	Taiwan SMART1	1.12	2.45	0.99	1.60	1.05	1.29	1.66	1.27	1.18

Fig. 25. Mean and standard deviation of surface settlement, $\bar{r}_{u,\text{peak}}$ and h_{liq} for different IMs, resulting from the UD and BD seismic shearing analyses with linearly scaled motions.

done separately for each of the three IMs, resulting in a total of six SFs per earthquake.

- For the BD shearing scenario, for each pair of ground motion a single SF was multiplied by both the x and y components such that the geometric mean of the IM of the scaled record matched the target value. Consequently, three SFs, one per IM, were derived per earthquake. The use of a geometric mean to combine the contributions of the x and y component is consistent with recommendations of the NRCC [70], and with the averaging type of the ground motion prediction equations used by Kramer and Mitchell [68].

The calculated SFs for each of the 20 new motions and each of the three IMs are presented in Table 7, both for the individual x and y components used for the unidirectional shearing analysis, and for the combined components used for the bidirectional shearing. The model configuration and soil properties used for this exercise were the same as those used in the development of the main dataset of the earlier sections. Table 8 summarizes the complete set of linearly scaled analyses related to the 2 (saturation conditions) × 1 (relative density) × 3 (loading directions) × 3 (target intensity measures) × 20 (pairs of ground motions) = 360 cases evaluated.

5.2. Role of target intensity measure

The results of the analyses were again evaluated in terms of surface settlement for the dry cases and $\bar{r}_{u,\text{peak}}$ and Δh_{liq} for the saturated models. Fig. 25 summarizes the results for each EDP, according to the different target IMs and from both UD and BD shearing analyses. Interestingly, the increase of the mean response of each EDP is consistent to what was obtained in the previous dataset: approximately 80% for

surface settlement, up to 30% for $\bar{r}_{u,\text{peak}}$ and around 6 m for h_{liq}. It is important to mention that these increases occur even when all the ground motions used in each approach, i.e., UD and BD shearing, were scaled to the same level of hazard, unlike the previous set of analyses which considered non-scaled motions. This evidence shows that scaling the recordings used in UD shearing analyses to any target IM is clearly not sufficient to account for the impact of BD seismic shearing, which is of essential practical importance. Note that the target IM is typically estimated in ground motion prediction equations as the geometric mean (or any variation) of the two horizontal components.

Fig. 25 also reveals that the choice of IM to characterize seismic hazard and to scale ground motions plays an important role in the predicted response and its variability. It can be observed that for all EDPs, PGA is the one IM yielding the largest and more uncertain results for either of the loading cases. It follows then that accounting for the impact of BD seismic shearing requires defining optimal ground motions intensity measures associated to both UD and BD seismic shearing. These optimal IMs would serve as ideal targets for scaling the earthquake recordings used as input in nonlinear dynamic analyses, for which there is an absence of geotechnical guidelines to account for multidirectional shaking effects. Existing research on optimal IMs for liquefaction-related phenomena at free-field conditions [e.g., 68,71], and for shallow foundations [e.g., 72,73], rely on UD shearing; thus, they need to be extended to consider BD seismic loading. It is likely then that, in the context of UD analysis and as long as such optimal IMs are used for scaling to the target hazard, additional SFs can be derived for considering the deleterious impact of BD shearing. These SFs would either a) increase the resulting excess pore water pressure and surface settlement, or b) amplify the UD load itself. Preliminary findings in terms of SFs to account for the BD seismic shearing in the *equivalent* UD analysis were presented by the authors in Adinata et al. [74]. The numerical methods used in the present paper can be further expanded to account for a more realistic soil stratigraphy, a range of soil properties, and even soil-structure interaction cases. Moreover, they can be used to develop validated procedures and/or guidelines for estimating soil response under BD seismic shearing.

6. Summary and conclusions

This paper quantified the impact of the multidirectional nature of ground motions on the shear-induced volumetric response during shaking for level ground sand deposits by means of a numerical approach. The series of non-linear dynamic analyses carried out for this purpose made use of a verified three-dimensional finite difference computer program for modeling dynamic wave propagation and solid-pore fluid interaction and an anisotropic bounding surface plasticity model for modeling the cyclic response of sands. The constitutive model was first validated against a number of bidirectional shearing centrifuge tests, showing the model predictive capabilities for capturing the shear-induced volumetric response in terms of excess pore water pressure and surface settlement during shaking. The numerical simulations consisted of modeling dry and fully water-saturated 30 m-deep sand deposits subjected to unidirectional (UD) and bidirectional (BD) seismic shearing. The analyses considered homogenous soil columns for three levels of relative density and different levels of shaking intensity. The results were evaluated in terms surface settlement for the case of the dry models and excess pore water pressure response during shaking for the saturated cases. For the saturated case surface settlement during shaking was negligible because the adopted hydraulic conductivity for the deposit that led to a nearly undrained response of the deposit. The comparison of the response of BD against the UD earthquake shaking showed the importance of accounting for both orthogonal components of ground motion in the horizontal plane rather than either one of those, as it was determined that the shear-induced volumetric response during BD seismic shearing is always higher. Specifically, the simulations revealed the following:

- For the dry deposits, the surface settlement was in average of 80% higher.
- In the saturated deposits, the depth-averaged peak excess pore water pressure ratio or $\bar{r}_{u,\text{peak}}$ was up to 60% higher. This increase proved to be larger for the case of dense sands ($D_\text{r} = 80\%$) deposit and smaller for the case of loose sands ($D_\text{r} = 30\%$) deposit.
- The thickness of the layer of soil approaching an $\bar{r}_{u,\text{peak}} = 1$ is in average 5–6 m larger in the 30 m-thick loose to medium dense soil deposits.

These results suggest that procedures to estimate volumetric strains and liquefaction-related phenomena require to account for BD seismic shearing as a closer approximation of realistic earthquake loading. An additional set of UD and BD shearing analyses which considered a target seismic hazard of a hypothetical site in Seattle, and relied on linear scaling, further showed the need for the development of optimal ground motions intensity measures for an adequate characterization and scaling of ground motions. Such intensity measures are key in developing in the development of validated methods and guidelines to address BD seismic shearing. These needs can be met by following the validated numerical methods used in developing the database introduced here and expanding them to more realistic scenarios.

The uncertainties of the results of the simulations conducted in this study are mostly related to the performance of the constitutive model, the deterministic characterization of its parameters, use of a constant hydraulic conductivity, and ground motion variability. Hence, the conclusions presented here can be further strengthen by considering spatial and temporal variation of material properties, deposit stratigraphy, and earthquakes from sub-crustal and subduction tectonic environments. Additionally, the understanding of the effects of BD seismic shearing should cover near-fault ground motions that exhibit directivity effects and direct interaction with the orientation of building structural elements.

Acknowledgements

References

[1] Pyke R, Seed HB, Chan CK. Settlement of sands under multidirectional shaking. Journal of the Geotechnical Engineering Division ASCE 1975;101(GT4):379–98.

[2] Seed HB, Pyke R, Martin GR. Effect of multidirectional shaking on pore pressure development in sands. Journal of Geotechnical and Geoenvironmental Engineering ASCE 1978;104(GT1):27–44.

[3] Martin GR, Finn WDL, Seed HB. Fundamentals of liquefaction under cyclic loading. Journal of the Geotechnical Engineering Division ASCE 1975;101(GT5):423–38.

[4] Tokimatsu K, Seed HB. Evaluation of settlements in sands due to earthquake shaking. Journal of Geotechnical Engineering 1987;113(8):861–78.

[5] Pradel D. Procedure to evaluate earthquake-induced settlements in dry sandy soils. J Geotech Geoenviron Eng 1998;124(4):364–8.

[6] Ishihara K, Yoshimine M. Evaluation of settlements in sand deposits following liquefaction during earthquakes. Soils Found 1992;32(1):173–88.

[7] Ishihara K, Yamazaki F. Cyclic simple shear tests on saturated sand in multi-directional loading. Soils Found 1980;20(1):45–59.

[8] Ishihara K, Nagase H. Multi-directional irregular loading tests on sand. Soil Dynam Earthq Eng 1988;7(4):201–12.

[9] Jones S, Sadrekarimi A. Effects of multi-directional and repeated loading on cyclic resistance of fraser river sand. Brandenberg SJ, Manzari MT, editors. Geotechnical earthquake engineering and soil dynamics V, vol. 293. ASCE: Geotechnical Special Publication; 2018. p. 247–56.

[10] Kammerer AM, Pestana JM, Seed RB. Undrained response of monterey 0/30 sand under multidirectional cyclic simple shear loading conditions, Geotechnical Engineering Report UCB/GT/02-01. Berkeley: University of California; 2002.

[11] Bhaumik L, Rutherford CJ, Cerna-Diaz A, Olson SM, Numanoglu OA, Hashash YMA, Weaver T. Volumetric strain in non-plastic silty sand subject to multidirectional cyclic loading. Brandon TL, Valentine RJ, editors. Geotechnical frontiers 2017, vol. 281. ASCE: Geotechnical Special Publication; 2017. p. 150–9.

[12] Su D, Li XS. Impact of multidirectional shaking on liquefaction potential of level sand deposits. Geotechnique 2008;58(4):259–67.

[13] El Shafee O, Abdoun T, Zeghal M. Centrifuge modelling and analysis of site liquefaction subjected to biaxial dynamic excitations. Geotechnique 2017;67(3):260–71.

[14] El Shafee O, Abdoun T, Zeghal M. Physical modeling and analysis of site liquefaction subjected to biaxial dynamic excitations. Innovative Infrastructure Solutions 2018;3(1):173–85.

[15] Cerna-Diaz A, Olson SM, Numanoglu OA, Hashash YMA, Bhaumik L, Rutherford CJ, Weaver T. Free-field cyclic response of dense sands in dynamic centrifuge tests with 1d and 2d shaking. Brandon TL, Valentine RJ, editors. Geotechnical frontiers 2017, vol. 281. Geotechnical Special Publication, ASCE; 2017. p. 121–30.

[16] Nie C-X, Chen Q-S, Gao G-Y, Yang J. Determination of seismic compression of sand subjected to two horizontal components of earthquake ground motions. Soil Dynam Earthq Eng 2016;92:330–3.

[17] Li XS, Wang ZL, Shen CK. Sumdes: a nonlinear procedure for response analysis of horizontally- layered sites subjected to multidirectional earthquake loading, Tech. Reps. Davis: Department of Civil Engineering, University of California; 1992http://nees.ucdavis.edu/Publications/reports/SUMDES-92.pdf.

[18] Wang ZL, Dafalias YF, Shen CK. Bounding surface hypoplasticity model for sand. J Eng Mech 1990;116(5):983–1001.

[19] Li XS, Dafalias YF. Dilatancy for cohesionless soils. Geotechnique 2000;50(4):448–60.

[20] Li XS. A sand model with state-dependent dilatancy. Geotechnique 2002;52(3):173–86.

[21] El Shamy U, Abdelhamid Y. Some aspects of the impact of multidirectional shaking on liquefaction of level and sloping granular deposits. J Eng Mech 2016;143(1):C4016003.

[22] Dashti S, Bray JD, Pestana JM, Riemer MF, Wilson D. Mechanisms of seismically induced settlement of buildings with shallow foundations on liquefiable soil. J Geotech Geoenviron Eng 2009;136(1):151–64.

[23] Itasca. FLAC3D: fast Lagrangian analysis of continua in 3 dimensions, version 5.01. Minneapolis, Minnesota, USA: Itasca Consulting Group Inc.; 2013.

[24] Biot MA. General theory of three-dimensional consolidation. J Appl Phys 1941;12:155–64.

[25] Detournay E, Cheng AD. Fundamentals of poroelasticity. Hudson JA, Fairhurst C, Brown ET, Hoek E, editors. Comprehensive rock engineering, vol. 2. Oxford, UK: Pergamon Press; 1993. p. 113–71. Ch. 5.

[26] Adinata J. Impact of bidirectional seismic shearing on volumetric response of sand deposits Canada: University of British Columbia, BC; 2018. Master's thesis.

[27] Tasiopoulou P, Taiebat M, Tafazzoli N, Jeremić B. Solution verification procedures for modeling and simulation of fully coupled porous media: static and dynamic behavior. Coupled System Mechanics 2015;4(1):67–98.

[28] Kwok AOL, Stewart JP, Hashash YMA, Matasovic N, Pyke R, Wang Z, Yang Z. Use of exact solutions of wave propagation problems to guide implementation of nonlinear seismic ground response analysis procedures. J Geotech Geoenviron Eng 2007;133(11):1385–98.

[29] Sarma SK. Analytical solution to the seismic response of visco-elastic soil layers. Geotechnique 1994;44(2):265–75.

[30] Roesset JM, Whitman RM. Theoretical background for amplification studies Cambridge, Massachusetts, USA: Massachusetts Institute of Technology; 1969. Research Report RR69-15.

[31] M. Yang, G. Seidalinov, M. Taiebat, Multidirectional cyclic shearing of clays and sands: evaluation of two bounding surface plasticity models, Soil Dynam Earthq Eng doi.org/10.1016/j.soildyn.2018.05.012.

[32] Manzari MT, Dafalias YF. A critical state two-surface plasticity model for sands. Geotechnique 1997;47(2):255–72.

[33] Dafalias YF, Manzari MT. Simple plasticity sand model accounting for fabric change effects. J Eng Mech 2004;130(6):622–34.

[34] Taiebat M, Dafalias YF. SANISAND: simple anisotropic sand plasticity model. Int J Numer Anal Methods Geomech 2008;32(8):915–48.

[35] Dafalias YF, Papadimitriou AG, Li X-S. Sand plasticity model accounting for inherent fabric anisotropy. J Eng Mech 2004;130(11):1319–33.

[36] Li XS, Dafalias YF. Anisotropic critical state theory: role of fabric. J Eng Mech 2012;138(3):263–75.

[37] Dafalias YF, Taiebat M. SANISAND-Z: zero elastic range sand plasticity model. Geotechnique 2016;66(12):999–1013.

[38] Barrero A. Multi-scale modeling of the response of granular soils under cyclic shearing Canada: University of British Columbia, BC; 2019. Ph.D. thesis.

[39] A. Ghofrani, P. Arduino, Prediction of leap centrifuge test results using a pressure-dependent bounding surface constitutive model, Soil Dynam Earthq Eng 113 (758-770).

[40] Ramirez J, Barrero AR, Chen L, Dashti S, Ghofrani A, Taiebat M, Arduino P. Site response in a layered liquefiable deposit: evaluation of different numerical tools and methodologies with centrifuge experimental results. J Geotech Geoenviron Eng 2018;144(10). 04018073.

[41] Been K, Jefferies MG. A state parameter for sands. Geotechnique 1985;35(2):99–112.

[42] Wood DM, Belkheir K, Liu DF. Strain softening and state parameter for sand modeling. Geotechnique 1994;42(2):335–9.

[43] Taiebat M, Shahir H, Pak A. Study of pore pressure variation during liquefaction using two constitutive models for sand. Soil Dynam Earthq Eng 2007;27(1):60–72.

[44] Taiebat M, Jeremić B, Dafalias YF, Kaynia AM, Cheng Z. Propagation of seismic waves through liquefied soils. Soil Dynam Earthq Eng 2010;30(4):236–57.

[45] Tasiopoulou P, Taiebat M, Tafazzoli N, Jeremić B. On validation of fully coupled behavior of porous media using centrifuge test results. Coupled System Mechanics 2015;4(1):37–65.

[46] Riemer MF. The effects of testing conditions on the constitutive behavior of loose, saturated sands under monotonic loading PhD. thesis Berkeley, California, USA: University of California; 1992.

[47] Wu J. Liquefaction triggering and post-liquefaction deformation of monterey 0/30 sand under uni-directional cyclic simple shear loading PhD. thesis Berkeley, California, USA: University of California; 2002.

[48] Su D, Ming HY, Li XS. Effect of shaking strength on the seismic response of lique-fiable level ground. Eng Geol 2013;166:262–71.

[49] Su D. Centrifuge investigation on responses of sand deposit and sand-pile system under multidirectional earthquake loading PhD. thesis China: Hong Kong University of Science and Tech- nology; 2005.

[50] Verdugo R, Ishihara K. The steady state of sandy soils. Soils Found 1996;36(2):81–91.

[51] Pradhan TB, Tatsuoka F, Sato Y. Experimental stress-dilatancy relations of sand subjected to cyclic loading. Soils Found 1989;29(1):45–64.

[52] Zhang JM, Shamoto Y, Tokimatsu K. Moving critical and phase-transformation stress state lines of saturated sand during undrained cyclic shear. Soils Found 1997;2(37):51–9.

[53] Scott R. Solidification and consolidation of a liquefied sand column. Soils Found 1986;26(4):23–31.

[54] Hushmand B, Crouse CB, Martin GR, Scott R. Site response and liquefaction studies involving the centrifuge. In: Cakmak AS, editor. Structures and stochastic methods, vol. 45 of development in geotechnical engineering. Elsevier Science; 1987. p. 3–24.

[55] Ishihara K. Review of the predictions for model 1 in the velacs program. Arulanandan K, Scott RF, editors. Verification of numerical procedures for the analysis of soil liquefaction problems, vol. 2. A.A. Balkema, The Netherland; 1994. p. 1353–9.

[56] Kim SR, Hwang JI, Ko HY, Kim MM. Development of dissipation model of excess pore pressure in liquefied sandy ground. J Geotech Geoenviron Eng 2009;135(4):544–54.

[57] Shahir H, Pak A, Taiebat M, Jeremić B. Evaluation of variation of permeability in liquefiable soil under earthquake loading. Comput Geotech 2012;40:74–88.

[58] Wang B, Zen K, Chen GQ, Zhang YB, Kasama K. Excess pore pressure dissipation and solidification after liquefaction of saturated sand deposits. Soil Dynam Earthq Eng 2013;49:157–64.

[59] El Shafee O. Physical and computational modeling of biaxial base excitation of sand deposits. Troy, NY, USA: Ph.D. thesis, Rensselaer Polytechnic Institute; 2016.

[60] Arulmoli K, Muraleetharan KK, Hosain MM, Fruth LS. Velacs laboratory testing program, soil data report, Technical Report 90-0562. Irvine, CA, Washington, DC, USA: The Earth Technology Corporation; March 1992.

[61] Kwan WS, Sideras SS, Kramer SL, Mohtar CE. Experimental database of cyclic simple shear tests under transient loadings. Earthq Spectra 2017;33(3):1219–39.

[62] Zeghal M, El Shafee O, Abdoun T. Analysis of soil liquefaction using centrifuge tests of a site subjected to biaxial shaking. Soil Dynam Earthq Eng 2018;114:229–41.

[63] McAllister G, Taiebat M, Ghofrani A, Chen L, Arduino P. Nonlinear site response analyses and high frequency dilation pulses. Proceedings of the sixty eighth Canadian geotechnical conference, quebec, QC, Canada. 2015. Paper ID: 447, 8 pages.

[64] Ancheta TD, Darragh RB, Stewart JP, Seyhan E, Silva WJ, Chiou BS-J, Wooddell KE, Graves RW, Kottke AR, Boore DM, Kishida T, Donahue JL. Peer nga-west2 database, PEER Report 2013/03. California, USA: Pacific Earthquake Engineering Research Center; 2013.

[65] Building Seismic Safety Council (BSCC). National earthquake hazard reduction program (NEHRP) recommended provisions for seismic regulations for new build-ings and other structures (Part 1: provisions, FEMA 450-1, and Part 2: commentary, FEMA 450-2). Washington, DC, USA: Federal Emergency Management Agency; 2003.

[66] Seed HB, Idriss IM. Simplified procedure for evaluating soil liquefaction potential. J Soil Mech Found Div 1971;107(SM9):1249–74.

[67] Kayen RE, Mitchell JK. Assessment of liquefaction potential during earthquakes by arias intensity. J Geotech Geoenviron Eng 1997;123:1162–74.

[68] Kramer SL, Mitchell RA. Ground motion intensity measures for liquefaction hazard evaluation. Earthq Spectra 2006;22(2):413–38.

[69] Bhaumik L, Cerna-Diaz A, Numanoglu OA, Olson SM, Rutherford CJ, Hashash YMA, Weaver T. Comparing shear response of dense sands from centrifuge and direct simple shear tests with published correlations. Brandenberg SJ, Manzari MT, edi-tors. Geotechnical earthquake engineering and soil dynamics V, vol. 293. Geotechnical Special Publication, ASCE; 2018. p. 122–31.

[70] National Research Council Canada (NRCC). National building code of Canada. fourteenth ed. Ottawa, ON, Canada: National Research Council; 2015.

[71] Dashti S, Karimi Z. Ground motion intensity measures to evaluate i: the liquefaction hazard in the vicinity of shallow-founded structures. Earthq Spectra 2017;33(1):241–76.

[72] Karimi Z, Dashti S. Ground motion intensity measures to evaluate ii: the perfor-mance of shallow-founded structures on liquefiable ground. Earthq Spectra 2017;33(1):277–98.

[73] Macedo J, Bray JD. Key trends in liquefaction-induced building settlement. J Geotech Geoenviron Eng 2018;144(11):04018076.

[74] Adinata J, Reyes A, Barrero AR, Taiebat M. An investigation on the effect of bi-directional seismic loading on volumetric strain and surface settlement of sand deposits. Brandenberg SJ, Manzari MT, editors. Geotechnical earthquake en-gineering and soil dynamics V, vol. 291. ASCE: Geotechnical Special Publication; 2018. p. 237–46.